

Revealing Hidden Substructures in the $M_{BH}-\sigma$ Diagram, and Refining the Bend in the $L-\sigma$ Relation

NANDINI SAHU,^{1,2} ALISTER W. GRAHAM² AND BENJAMIN L. DAVIS²

¹*OzGrav-Swinburne, Centre for Astrophysics and Supercomputing, Swinburne University of Technology, Hawthorn, VIC 3122, Australia*

²*Centre for Astrophysics and Supercomputing, Swinburne University of Technology, Hawthorn, VIC 3122, Australia*

(Accepted 2019 October 22, by The Astrophysical Journal)

ABSTRACT

Using 145 early- and late-type galaxies (ETGs and LTGs) with directly-measured super-massive black hole masses, M_{BH} , we build upon our previous discoveries that: (i) LTGs, most of which have been alleged to contain a pseudobulge, follow the relation $M_{BH} \propto M_{*,sph}^{2.16 \pm 0.32}$; and (ii) the ETG relation $M_{BH} \propto M_{*,sph}^{1.27 \pm 0.07}$ is an artifact of ETGs with/without disks following parallel $M_{BH} \propto M_{*,sph}^{1.9 \pm 0.2}$ relations which are offset by an order of magnitude in the M_{BH} -direction. Here, we searched for substructure in the M_{BH} –(central velocity dispersion, σ) diagram using our recently published, multi-component, galaxy decompositions; investigating divisions based on the presence of a depleted stellar core (major dry-merger), a disk (minor wet/dry-merger, gas accretion), or a bar (evolved unstable disk). The Sérsic and core-Sérsic galaxies define two distinct relations: $M_{BH} \propto \sigma^{5.75 \pm 0.34}$ and $M_{BH} \propto \sigma^{8.64 \pm 1.10}$, with $\Delta_{rms|BH} = 0.55$ and 0.46 dex, respectively. We also report on the consistency with the slopes and bends in the galaxy luminosity (L)– σ relation due to Sérsic and core-Sérsic ETGs, and LTGs which all have Sérsic light-profiles. Two distinct relations (superficially) reappear in the M_{BH} – σ diagram upon separating galaxies with/without a disk (primarily for the ETG sample), while we find no significant offset between barred and non-barred galaxies, nor between galaxies with/without active galactic nuclei. We also address selection biases purported to affect the scaling relations for dynamically-measured M_{BH} samples. Our new, (morphological type)-dependent, M_{BH} – σ relations more precisely estimate M_{BH} in other galaxies, and hold implications for galaxy/black hole co-evolution theories, simulations, feedback, the pursuit of a black hole fundamental plane, and calibration of virial f -factors for reverberation-mapping.

Keywords: black hole physics — galaxies: evolution — galaxies: kinematics and dynamics — galaxies: elliptical and lenticular, cD — galaxies: spiral — galaxies: structure

1. INTRODUCTION

The first observational works on the correlation between central black hole mass (M_{BH}) and the stellar velocity dispersion (σ) of a galaxy (Ferrarese & Merritt 2000; Gebhardt et al. 2000) revealed a relation with little or no intrinsic scatter, suggesting that the M_{BH} – σ relation could be the most fundamental of the black hole scaling relations. However, surprisingly, the slopes reported by the two studies were not in agreement

and supported two competing feedback models between the super-massive black holes (SMBHs) and their host galaxies. Ferrarese & Merritt (2000) found $M_{BH} \propto \sigma^{4.80 \pm 0.50}$, which supported the prediction $M_{BH} \propto \sigma^5$ based on the energy-balancing feedback model of Silk & Rees (1998). Gebhardt et al. (2000) reported $M_{BH} \propto \sigma^{3.75 \pm 0.30}$, supporting the feedback model of Fabian (1999) based upon momentum conservation, which predicted $M_{BH} \propto \sigma^4$.

Merritt & Ferrarese (2001) later revealed that Gebhardt et al. (2000) had found a shallower slope due to the asymmetric linear regression routine that

Gebhardt et al. (2000) employed¹, plus Gebhardt et al.’s relation was biased by the low-velocity dispersion which they had used for the Milky Way. Gebhardt et al. (2000) had effectively solved the “Observer’s Question” while Ferrarese & Merritt (2000) had effectively answered the “Theorist’s Question,” as was later posed by Novak et al. (2006). The reason behind obtaining almost zero intrinsic scatter in the $M_{BH}-\sigma$ relation was possibly the small sample size, or perhaps Ferrarese & Merritt (2000) had a “gold standard” of reliable black hole masses with well-resolved spheres-of-influence (Ferrarese & Ford 2005). Subsequent works on larger galaxy samples have found a non-zero intrinsic scatter.

With an increase in the number of barred galaxies with directly measured SMBH masses, some studies (Graham 2007, 2008a,b; Hu 2008) found that barred galaxies have a tendency to be offset, from the $M_{BH}-\sigma$ relation, towards higher σ or lower M_{BH} , suggesting that the inclusion of barred galaxies may produce a steeper relation with larger scatter as warned by (Graham et al. 2011) and (Graham & Scott 2013). Hu (2008) claimed that the offset galaxies in their sample had “pseudo-bulges”² with low-mass black holes, while according to Graham (2008b), the offset could be either because of a low black hole mass in pseudo-bulges or the elevated velocity dispersions in barred galaxies. Supporting the latter possibility, the simulation by Hartmann et al. (2014) suggested that bars may cause increased velocity dispersion in galactic bulges whether they are classical or pseudo-bulges (see also Brown et al. 2013). Interestingly, the recent observational work by Sahu et al. (2019) found that barred galaxies are not offset in the black hole mass versus galaxy stellar mass ($M_{*,gal}$) diagram, nor in the black hole mass versus spheroid/bulge stellar mass ($M_{*,sph}$) diagram, eliminating under-massive black holes as the reason behind the apparent offset in the $M_{BH}-\sigma$ diagram and strengthening the prospect of barred galaxies having an increased velocity dispersion. However, as the number of barred galaxies in Sahu et al. (2019) is

still quite small, this interpretation may require further confirmation.

In addition to the reported substructure in the $M_{BH}-\sigma$ diagram due to barred galaxies, some studies (e.g., McConnell & Ma 2013; Bogdán et al. 2018, see their figure 5) have noticed that massive galaxies are offset towards the high- M_{BH} side of their $M_{BH}-\sigma$ relation. These galaxies are mostly brightest cluster galaxies (BCGs) or central cluster galaxies (CCGs) which are considered to be a product of multiple dry mergers. Galaxies which have undergone dry mergers can have a deficit of light at their centers because the binary SMBHs formed from the two merging galaxies can scour out the stars from the center of the merged galaxy through the transfer of their orbital angular momentum (Begelman et al. 1980; Merritt & Milosavljević 2005). Such galaxies with a (partially) depleted core were discovered by King & Minkowski (1966, 1972) and are referred to as core-Sérsic (Graham et al. 2003) galaxies due to their flattened core relative to the inward extrapolation of their bulge’s outer Sérsic (Sérsic 1963) light profile. Galaxies which grow over time via gas-rich processes are likely to have bulges with Sérsic light profiles.

Contrary to McConnell & Ma (2013), the recent work by Savorgnan & Graham (2015) found that Sérsic and core-Sérsic galaxies broadly follow the same $M_{BH}-\sigma$ relation, and so was the case with slow and fast rotating galaxies in their sample. Thus, still, debates over the substructures in the $M_{BH}-\sigma$ diagram due to barred and non-barred galaxies, Sérsic and core-Sérsic galaxies, and fast and slow rotating galaxies (galaxies with and without a rotating disk) persist.

Using the hitherto largest sample of 144 galaxies, comprised of all early-type galaxies (ETGs) and late-type galaxies (LTGs) with directly measured SMBH masses, our work investigates the underlying relationship between black hole mass and central velocity dispersion for various sub-classes of the host galaxy. We classify these galaxies into Sérsic, core-Sérsic, barred, non-barred, and galaxies with and without a disk, based on our detailed multi-component decompositions (coupled with kinematical information) presented in Davis et al. (2019) and Sahu et al. (2019), and also into galaxies with and without an Active Galactic Nucleus (AGN) identified using the catalog of Véron-Cetty & Véron (2010).

We endeavor here to build upon our recent revelation that ETGs superficially follow the relation $M_{BH} \propto M_{*,sph}^{1.27 \pm 0.07}$ (Sahu et al. 2019, their Equation 10). We showed in Sahu et al. (2019, see their Figure 8) that this single relation for ETGs is misleading because ETGs with and without a disk define two separate (parallel)

¹ Tremaine et al. (2002) also used an asymmetric linear regression, ignoring the intrinsic scatter in the velocity dispersion direction (see Novak et al. 2006; Graham 2016, his section titled “slippery slopes”).

² Pseudo-bulges are difficult to identify (Graham 2014), and Graham (2019a) explains why diagrams using Sérsic indices and “effective” half-light parameters cannot be used to identify pseudo-bulges. Moreover, the range of diagnostics used to classify pseudo-bulges need to be subjectively applied (Kormendy & Kennicutt 2004), making it extremely problematic to distinguish pseudo-bulges from classical bulges. Furthermore, many galaxies contain both (Erwin et al. 2015).

$M_{BH} \propto M_{*,sph}^{1.9 \pm 0.2}$ relations which are offset by more than an order of magnitude (1.12 dex) in the M_{BH} -direction. This paradigm shifting discovery provided further impetus for us to re-examine old and search for new sub-structure in the $M_{BH}-\sigma$ diagram.

In order to provide a consistency check between the various scaling relations, this paper also establishes the galaxy luminosity (L)- σ relation for our ETG sample observed at $3.6 \mu\text{m}$, and for an updated V-band dataset of ETGs (Lauer et al. 2007). We find a bend in the ETG $L-\sigma$ relation from both data-sets, which has been observed in other bands (e.g., Matković & Guzmán 2005; de Rijcke et al. 2005; Graham & Soria 2019). Additionally, we explore the behavior of LTGs (spirals) with directly measured black hole masses in the $L-\sigma$ diagram. We mate these $L-\sigma$ relations with the $M_{BH}-L$ and $M_{BH}-\sigma$ relations to investigate the consistency between the scaling relations.

Section 2 describes our data-set. In Section 3, we briefly discuss the method of linear regression that we have used to establish our scaling relations, and the galaxy exclusions applied, along with the reasons for this. We further present the new $M_{BH}-\sigma$ relations that we have found for the various categories based on the morphological classes mentioned above. This is accompanied by discussions on the behavior of the $M_{BH}-\sigma$ relation for each category.

In Section 4, we check on the internal consistency between our $M_{BH}-\sigma$ relations and the latest $M_{BH}-M_{*,gal}$ (and $M_{BH}-M_{*,sph}$) relations, while Section 5 presents the bent $L-\sigma$ relations, based on different wavelength bands. Section 6 addresses a much-discussed selection bias regarding the spatial-resolution of the gravitational sphere-of-influence of the black holes, and investigates the previously observed offset between galaxies with a dynamically measured black hole mass and galaxies without a dynamically measured black hole mass in the $L-\sigma$, or rather $\sigma-M_{*,gal}$, diagram (Shankar et al. 2016). This is followed by the main conclusions of our work summarized in Section 7 and a brief discussion on the implications of the new scaling relations.

2. DATA

We have identified 145 galaxies with directly measured super-massive black hole masses obtained from stellar dynamics, gas dynamics, kinematics of megamasers, proper motion, or recent direct imaging technique. This sample is comprised of 96 early-type and 49 late-type galaxies. Data for 84 ETGs came from Sahu et al. (2019) and Savorgnan et al. (2016). These 84 ETGs have been used in Sahu et al. (2019) to establish the $M_{BH}-M_{*,sph}$ and $M_{BH}-M_{*,gal}$ relations for

ETGs, based on the bulge and total galaxy stellar masses measured using state-of-the-art two dimensional (2D) isophotal modelling^{3,4} and multi-component decompositions of predominantly near infra-red (NIR) images.

For the remaining 12 ETGs, data for two galaxies came from Nowak et al. (2007) and Gültekin et al. (2014), who measured M_{BH} using stellar dynamics. Another galaxy is taken from Huré et al. (2011) with M_{BH} measured using water masers, while the data for the remaining nine ETGs is taken from recent papers. Out of these nine, two ETGs are from Nguyen et al. (2018) and six ETGs come from Thater et al. (2019), where M_{BH} is measured using stellar dynamics. Data for the last ETG is taken from Boizelle et al. (2019) who measured M_{BH} using gas dynamics.

Data for 44 of the 49 LTGs (spiral galaxies) is taken from Davis et al. (2018) and Davis et al. (2019), where they also present the $M_{BH}-M_{*,sph}$, $M_{BH}-M_{*,disk}$, and $M_{BH}-M_{*,gal}$ relations for spiral galaxies based on predominantly NIR imaging and multi-component decompositions. Out of the remaining five LTGs, four are taken from Combes et al. (2019), and one from Nguyen et al. (2019), where the central SMBH masses have been measured using gas dynamics.

Our galaxy sample is listed in Table 1, which includes information on the galaxy type, distance, updated morphology, presence of a bar, disk, depleted stellar core, AGN, M_{BH} , and the central stellar velocity dispersion. The morphologies reflect the presence, or not, of an intermediate or large-scale disk, and also bar, with types designated by the morphological galaxy classification grid given by Graham (2019a).

The velocity dispersion has been measured in many ways in literature, for example: luminosity-weighted line-of-sight stellar velocity dispersion within one ef-

³ Davis et al. (2019) and Sahu et al. (2019) use ISOFIT (Ciambur 2015) to generate a 2D model of each galaxy, and further use PROFILER (Ciambur 2016) to effectively realign the semi-major axis of each isophote. This 1D surface brightness profile effectively encapsulates all of the key information about the galaxy structure and flux, including ellipticity gradients, position angle twists, and deviations from elliptical-shaped isophotes up to the 12th order Fourier harmonic coefficients. This major axis surface brightness profile is used for multi-component decomposition of the galaxy light. It should not be confused with a simple surface brightness profile obtained from a 1D cut of a galaxy image.

⁴ Ciambur (2016) provide a critical comparison between 1D and 2D decomposition techniques, concluding that multi-component galaxies may be easily modelled in 2D but gradients in the ellipticity, position angle, and structural perturbations are better captured in 1D. Furthermore, Savorgnan & Graham (2016) tried both 1D and 2D decompositions, and had more success using the 1D multi-component decomposition techniques.

fective radius ($R_{e, sph}$) of the spheroid $\sigma_{e, sph}$ (e.g., Gebhardt et al. 2000); luminosity-weighted line-of-sight stellar rotation and velocity dispersion (added in quadrature) within one effective radius of either the spheroid ($R_{e, sph}$) or the whole galaxy ($R_{e, gal}$) (Gültekin et al. 2009a); or velocity dispersions within an aperture of radius equal to one-eighth⁵ of $R_{e, sph}$, $\sigma_{e/8}$ (e.g., Ferrarese & Merritt 2000).

It should be noted that the effective radius of the spheroid and the effective radius of the whole galaxy are, in general, different quantities. Velocity dispersions measured using an aperture size equal to the effective radius of a galaxy is highly prone to contamination from the kinematics of the stellar disk in those galaxies with a (large-scale or intermediate-scale) disk. Whereas, studies (e.g., Gültekin et al. 2009b) which use the luminosity-weighted average of both the stellar rotation and the velocity dispersion certainly represent a biased velocity dispersion. The use of the effective radius of the spheroid (bulge) as a scale of aperture size is also precarious as the measured velocity dispersion may also have contributions from the disk. Moreover, $R_{e, sph}$ does not have any physical significance, see Graham (2019b) for a detailed study on $R_{e, sph}$. The introduction of radii containing 50% of the light reflects an arbitrary and physically meaningless percentage. The use of a different percentage, x , results in R_e/R_x ratios that systematically change with luminosity, and in turn σ_e/σ_x changes. There is nothing physically meaningful with σ_e , and $M_{BH}-\sigma_x$ relations are a function of the arbitrary percentage x .

Bennert et al. (2015, their Figure 1) compare velocity dispersions based on different aperture sizes ($R_{e, sph}, R_{e, sph}/8, R_{e, gal}$) and conclude that different methods may produce velocity dispersion values different by up to 40%. However, for most of their sample, the agreement between σ_{SDSS} (aperture size $R_{e, sph}/8$) and their $\sigma_{e, sph}$ (aperture size $R_{e, sph}$) values is much better than 40%. The radial variation of aperture velocity dispersions are a weak function of radius for ETGs, e.g., $\sigma_R = \sigma_e \times (R/R_e)^{-0.04}$ (Jorgensen et al. 1995), and $\sigma_R = \sigma_e \times (R/R_e)^{-0.066}$ (Cappellari et al. 2006).

These empirical relations explain the reasonable agreement between σ based on different apertures, however this might be true only for simple ETGs. Whereas for multi-component (barred-ETG, spiral) galaxies, σ measurements are more complicated and large aperture sizes can introduce significant errors.

Given the inconsistency in the use of aperture size and contamination due to both disk rotation and velocity dispersion when using a large aperture size, we use the central velocity dispersion. Moreover, such data exists. The central velocity dispersions for the majority of our galaxies are taken from the HYPERLEDA database⁶ (Paturel et al. 2003), as of October 2019. Galaxies for which we obtained velocity dispersions from other sources are indicated in Table 1. Velocity dispersions obtained from the HYPERLEDA database are homogenized for a uniform aperture size of $0.595 \text{ h}^{-1} \text{ kpc}$.

A source of error in the measured central velocity dispersions is broad line region (BLR) emission from AGNs and the movement of stars within the central black hole’s sphere-of-influence. However, as our central velocity dispersions are based on an aperture size a few hundred times the typical radial extent of the sphere-of-influence, which is a few parsecs, the contamination in the luminosity-weighted velocity dispersion will be minimal.

In the past, velocity dispersion observations have been obtained using long-slit spectroscopy. Nowadays, we can get better measurements using integral field spectrographs equipped with Integral Field Units (IFUs), where a spatially resolved 2D spectrum gives an accurate measurement of the stellar velocity dispersion of a galaxy. However, this measurement is not available for most of our galaxy sample; hence, we proceed with the central velocity measurements available on HYPERLEDA.

For the majority of galaxies in our sample, the uncertainty in the velocity dispersion reported by HYPERLEDA is $\lesssim 10\%$. Given that seeing and slit orientation can influence the measured velocity dispersion, we use a constant uncertainty of 10%, whereas, for M_{BH} , we use the errors provided by the references, listed in Table 1. In addition, we check the robustness of our $M_{BH}-\sigma$ relations by using a 5% to 15% uncertainty on σ .

⁵ The velocity dispersion measurements available in Sloan Digital Sky Survey (SDSS) database use this aperture size.

⁶ <http://leda.univ-lyon1.fr/leda/param/vdis.html>

Table 1. Galaxy Sample

Galaxy	Type	Distance	Morph	Bar	Disk	Core	AGN	$\log(M_{BH}/M_{\odot})$	Source	$\log(\sigma/\text{km s}^{-1})$
(1)	(2)	(3)	(4)	(5)	(6)	(7)	(8)	(9)	(10)	(11)
		(Mpc)						(dex)		(dex)
IC 1459	ETG	28.4	E	no	no	yes	yes	9.38 ± 0.20 [S]	SG(2016)	2.47
NGC 0821	ETG	23.4	E	no	no	no	no	7.59 ± 0.17 [S]	SG(2016)	2.30
NGC 1023	ETG	11.1	S0-bar	yes	yes	no	no	7.62 ± 0.05 [S]	SG(2016)	2.29
NGC 1316	ETG	18.6	SAB0 (merger)	yes	yes	no	no	8.18 ± 0.26 [S]	SG(2016)	2.35
NGC 1332	ETG	22.3	ES	no	yes	no	no	9.16 ± 0.07 [S]	SG(2016)	2.47
NGC 1399	ETG	19.4	E	no	no	yes	no	8.67 ± 0.06 [S]	SG(2016)	2.52
NGC 2549	ETG	12.3	S0	yes	yes	no	no	7.15 ± 0.60 [S]	SG(2016)	2.15
NGC 2778	ETG	22.3	S0	yes	yes	no	no	7.18 ± 0.34 [S]	SG(2016)	2.19
NGC 3091	ETG	51.2	E	no	no	yes	no	9.56 ± 0.04 [S]	SG(2016)	2.49
NGC 3115	ETG	9.4	S0	no	yes	no	no	8.94 ± 0.25 [S]	SG(2016)	2.42
NGC 3245	ETG	20.3	S0	yes	yes	no	no	8.30 ± 0.12 [G]	SG(2016)	2.32
NGC 3377	ETG	10.9	E	no	no	no	no	7.89 ± 0.04 [S]	SG(2016)	2.13
NGC 3379 (M 105)	ETG	10.3	E	no	no	yes	no	8.60 ± 0.12 [S]	SG(2016)	2.31
NGC 3384 ^a	ETG	11.3	S0	yes	yes	no	no	7.23 ± 0.05 [S]	SG(2016)	2.16
NGC 3414	ETG	24.5	E	no	no	no	no	8.38 ± 0.06 [S]	SG(2016)	2.38
NGC 3489 ^a	ETG	11.7	S0	yes	yes	no	no	6.76 ± 0.07 [S]	SG(2016)	2.02
NGC 3585	ETG	19.5	E	no	no	no	no	8.49 ± 0.13 [S]	SG(2016)	2.33
NGC 3607	ETG	22.2	E	no	no	no	yes	8.11 ± 0.18 [S]	SG(2016)	2.35
NGC 3608	ETG	22.3	E	no	no	yes	no	8.30 ± 0.18 [S]	SG(2016)	2.29
NGC 3842	ETG	98.4	E	no	no	yes	no	9.99 ± 0.13 [S]	SG(2016)	2.49
NGC 3998	ETG	13.7	S0	yes	yes	no	yes	8.91 ± 0.11 [S]	SG(2016)	2.42
NGC 4261	ETG	30.8	E	no	no	yes	yes	8.70 ± 0.09 [S]	SG(2016)	2.47
NGC 4291	ETG	25.5	E	no	no	yes	no	8.52 ± 0.36 [S]	SG(2016)	2.47
NGC 4374 (M 84)	ETG	17.9	E	no	no	yes	yes	8.95 ± 0.05 [S]	SG(2016)	2.44
NGC 4459	ETG	15.7	S0	no	yes	no	no	7.83 ± 0.09 [G]	SG(2016)	2.24
NGC 4472 (M 49)	ETG	17.1	E	no	no	yes	yes	9.40 ± 0.05 [S]	SG(2016)	2.45
NGC 4473	ETG	15.3	E	no	no	no	no	8.08 ± 0.36 [S]	SG(2016)	2.25
NGC 4486 (M 87)	ETG	16.8	E	no	no	yes	yes	9.81 ± 0.05 [DI] ^b	SG(2016)	2.51
NGC 4564	ETG	14.6	S0	no	yes	no	no	7.78 ± 0.06 [S]	SG(2016)	2.19
NGC 4596	ETG	17.0	S0	yes	yes	no	no	7.90 ± 0.20 [G]	SG(2016)	2.15
NGC 4621 (M 59)	ETG	17.8	E	no	no	no	no	8.59 ± 0.05 [S]	SG(2016)	2.36
NGC 4697	ETG	11.4	E	no	no	no	no	8.26 ± 0.05 [S]	SG(2016)	2.22
NGC 4889	ETG	103.2	E	no	no	yes	no	10.32 ± 0.44 [S]	SG(2016)	2.59
NGC 5077	ETG	41.2	E	no	no	yes	yes	8.87 ± 0.22 [G]	SG(2016)	2.40
NGC 5128	ETG	3.8	S0 (merger)	no	yes	no	no	7.65 ± 0.13 [SG]	SG(2016)	2.01
NGC 5576	ETG	24.8	E	no	no	no	no	8.20 ± 0.10 [S]	SG(2016)	2.26
NGC 5846	ETG	24.2	E	no	no	yes	no	9.04 ± 0.05 [S]	SG(2016)	2.38
NGC 6251	ETG	104.6	E	no	no	yes	yes	8.77 ± 0.16 [G]	SG(2016)	2.49
NGC 7619	ETG	51.5	E	no	no	yes	no	9.40 ± 0.09 [S]	SG(2016)	2.50
NGC 7768	ETG	112.8	E	no	no	yes	no	9.11 ± 0.15 [S]	SG(2016)	2.46
NGC 1271	ETG	80.0	ES	no	yes	no	no	9.48 ± 0.16 [S]	GCS(2016)	2.44 [11a]
NGC 1277	ETG	72.5	ES	no	yes	no	no	9.08 ± 0.12 [S]	G+7(2016)	2.48 [11b]
A1836 BCG	ETG	158.0	E	no	no	yes	no	9.59 ± 0.06 [G]	SGD(2019)	2.49[11c]
A3565 BCG (IC 4296)	ETG	40.7	E	no	no	no	yes	9.04 ± 0.09 [G]	SGD(2019)	2.52
Mrk 1216	ETG	94.0	S0	no	yes	no	yes	9.69 ± 0.16 [S]	SGD(2019)	2.51
NGC 0307	ETG	52.8	SAB0	yes	yes	no	no	8.34 ± 0.13 [S]	SGD(2019)	2.43
NGC 0404	ETG	3.1	S0	no	yes	no	no	4.85 ± 0.13 [S]	SGD(2019)	1.54
NGC 0524	ETG	23.3	SA0(rs)	no	yes	yes	no	8.92 ± 0.10 [S]	SGD(2019)	2.37
NGC 1194	ETG	53.2	S0 (merger?)	no	yes	no	yes	7.81 ± 0.04 [M]	SGD(2019)	2.17 [11d]
NGC 1275	ETG	72.9	E	no	no	no	yes	8.90 ± 0.20 [G]	SGD(2019)	2.39

Table 1 continued

Table 1 (*continued*)

Galaxy	Type	Distance	Morph	Bar	Disk	Core	AGN	$\log(M_{BH}/M_{\odot})$	Source	$\log(\sigma/\text{km s}^{-1})$
(1)	(2)	(3)	(4)	(5)	(6)	(7)	(8)	(9)	(10)	(11)
		(Mpc)						(dex)		(dex)
NGC 1374	ETG	19.2	S0	no	yes	no	no	8.76 ± 0.05 [S]	SGD(2019)	2.25
NGC 1407	ETG	28.0	E	no	no	yes	no	9.65 ± 0.08 [S]	SGD(2019)	2.42
NGC 1550	ETG	51.6	E	no	no	yes	no	9.57 ± 0.06 [S]	SGD(2019)	2.48
NGC 1600	ETG	64.0	E	no	no	yes	no	10.23 ± 0.05 [S]	SGD(2019)	2.52
NGC 2787	ETG ^a	7.3	SB0(r)	yes	yes	no	yes	7.60 ± 0.06 [G]	SGD(2019)	2.28
NGC 3665	ETG	34.7	S0	no	yes	no	no	8.76 ± 0.10 [G]	SGD(2019)	2.33
NGC 3923	ETG	20.9	E	no	no	yes	no	9.45 ± 0.13 [S]	SGD(2019)	2.39
NGC 4026	ETG	13.2	SB0	yes	yes	no	no	8.26 ± 0.11 [S]	SGD(2019)	2.24
NGC 4339	ETG	16.0	S0	no	yes	no	no	7.63 ± 0.33 [S]	SGD(2019)	2.05
NGC 4342	ETG	23.0	ES	no	yes	no	no	8.65 ± 0.18 [S]	SGD(2019)	2.38
NGC 4350	ETG	16.8	EBS	yes	yes	no	no	8.86 ± 0.41 [SG]	SGD(2019)	2.26
NGC 4371 ^a	ETG	16.9	SB(r)0	yes	yes	no	no	6.85 ± 0.08 [S]	SGD(2019)	2.11
NGC 4429	ETG	16.5	SB(r)0	yes	yes	no	no	8.18 ± 0.09 [G]	SGD(2019)	2.24
NGC 4434	ETG	22.4	S0	no	yes	no	no	7.85 ± 0.17 [S]	SGD(2019)	2.07
NGC 4486B	ETG	15.3	E	no	no	no	no	8.76 ± 0.24 [S]	SGD(2019)	2.22
NGC 4526	ETG	16.9	S0	no	yes	no	no	8.67 ± 0.05 [G]	SGD(2019)	2.35
NGC 4552	ETG	14.9	E	no	no	no	yes	8.67 ± 0.05 [S]	SGD(2019)	2.40
NGC 4578	ETG	16.3	S0(r)	no	yes	no	no	7.28 ± 0.35 [S]	SGD(2019)	2.05
NGC 4649	ETG	16.4	E	no	no	yes	no	9.67 ± 0.10 [S]	SGD(2019)	2.52
NGC 4742	ETG	15.5	S0	no	yes	no	no	7.15 ± 0.18 [S]	SGD(2019)	2.01
NGC 4751	ETG	26.9	S0	no	yes	yes	no	9.15 ± 0.05 [S]	SGD(2019)	2.54
NGC 4762	ETG	22.6	SB0	yes	yes	no	no	7.36 ± 0.15 [S]	SGD(2019)	2.15
NGC 5018	ETG	40.6	S0 (merger)	no	yes	no	no	8.02 ± 0.09 [S]	SGD(2019)	2.33
NGC 5252	ETG	96.8	S0	no	yes	no	yes	9.00 ± 0.40 [G]	SGD(2019)	2.27
NGC 5328	ETG	64.1	E	no	no	yes	no	9.67 ± 0.15 [S]	SGD(2019)	2.50
NGC 5419	ETG	56.2	E	no	no	yes	no	9.86 ± 0.14 [S]	SGD(2019)	2.54
NGC 5516	ETG	58.4	E	no	no	yes	no	9.52 ± 0.06 [S]	SGD(2019)	2.49
NGC 5813	ETG	31.3	S0	no	yes	yes	no	8.83 ± 0.06 [S]	SGD(2019)	2.37
NGC 5845	ETG	25.2	ES	no	yes	no	no	8.41 ± 0.22 [S]	SGD(2019)	2.36
NGC 6086	ETG	138.0	E	no	no	yes	no	9.57 ± 0.17 [S]	SGD(2019)	2.51
NGC 6861	ETG	27.3	ES	no	yes	no	no	9.30 ± 0.08 [S]	SGD(2019)	2.59
NGC 7052	ETG	66.4	E	no	no	yes	no	8.57 ± 0.23 [G]	SGD(2019)	2.45
NGC 7332	ETG	24.9	SB0	yes	yes	no	no	7.11 ± 0.20 [S]	SGD(2019)	2.11
NGC 7457	ETG	14.0	S0	no	yes	no	no	7.00 ± 0.30 [S]	SGD(2019)	1.83
NGC 4486A	ETG	13.9	E	no	no	no	no	7.10 ± 0.32 [S]	No+7(2007)	2.12
NGC 5102	ETG	3.2	S0	no	yes	no	no	5.94 ± 0.38 [S]	Ngu+10(2018)	1.79
NGC 5206	ETG	3.5	dE/dS0	no	no?	no	no	5.67 ± 0.36 [S]	Ngu+10(2018)	1.62
NGC 0584	ETG	19.1	S0	no	yes	yes	no	8.11 ± 0.18 [S]	Th+6(2019)	2.33 [11e]
NGC 2784	ETG	9.6	S0	no	yes	no	no	8.00 ± 0.31 [S]	Th+6(2019)	2.39 [11e]
NGC 3640	ETG	26.3	E	no	no	yes	no	7.89 ± 0.34 [S]	Th+6(2019)	2.24 [11e]
NGC 4281	ETG	24.4	S0	no	yes	no	no	8.73 ± 0.08 [S]	Th+6(2019)	2.50 [11e]
NGC 4570	ETG	17.1	S0	no	yes	no	no	7.83 ± 0.14 [S]	Th+6(2019)	2.32 [11e]
NGC 7049	ETG	29.9	S0	no	yes	no	no	8.51 ± 0.12 [S]	Th+6(2019)	2.42 [11e]
NGC 3258	ETG	31.3	E	no	no	yes	no	9.35 ± 0.05 [G]	Bo+7(2019)	2.41
IC 1481	ETG	89.9	E? (merger)	7.15 ± 0.13 [S]	Hu+4(2011)	...
NGC 3706	ETG	46	S0	no	yes	yes	no	8.78 ± 0.06 [S]	Gu+6(2014)	2.41
Circinus ^a	LTG	4.2	SABb	no	yes	no	yes	6.25 ± 0.11 [M]	DGC(2019)	2.17
Cygnus A	LTG	258.8	S	no	yes	no	yes	9.44 ± 0.13 [G]	DGC(2019)	2.43 [11f]
ESO558-G009 ^a	LTG	115.4	Sbc	no	yes	no	no	7.26 ± 0.04 [M]	DGC(2019)	2.23 [11g]
IC 2560 ^a	LTG	31.0	SBb	yes	yes	no	yes	6.49 ± 0.20 [M]	DGC(2019)	2.14
J0437+2456 ^a	LTG	72.8	SB	yes	yes	no	no	6.51 ± 0.05 [M]	DGC(2019)	2.04 [11g]

Table 1 *continued*

Table 1 (*continued*)

Galaxy	Type	Distance	Morph	Bar	Disk	Core	AGN	$\log(M_{BH}/M_{\odot})$	Source	$\log(\sigma/\text{km s}^{-1})$
(1)	(2)	(3)	(4)	(5)	(6)	(7)	(8)	(9)	(10)	(11)
		(Mpc)						(dex)		(dex)
Milky Way ^a	LTG	7.9	SBbc	yes	yes	no	no	6.60 ± 0.02 [P]	DGC(2019)	2.02 [11f]
Mrk 1029 ^a	LTG	136.9	S	no	yes	no	no	6.33 ± 0.12 [M]	DGC(2019)	2.12 [11g]
NGC 0224	LTG	0.8	SBb	yes	yes	no	no	8.15 ± 0.16 [S]	DGC(2019)	2.19
NGC 0253 ^a	LTG	3.5	SABc	yes	yes	no	no	7.00 ± 0.30 [G]	DGC(2019)	1.98
NGC 1068 ^a	LTG	10.1	SBb	yes	yes	no	yes	6.75 ± 0.08 [M]	DGC(2019)	2.21
NGC 1097 ^a	LTG	24.9	SBb	yes	yes	no	yes	8.38 ± 0.04 [G]	DGC(2019)	2.29 [11h]
NGC 1300 ^a	LTG	14.5	SBbc	yes	yes	no	no	7.71 ± 0.16 [G]	DGC(2019)	2.34
NGC 1320 ^a	LTG	37.7	Sa	no	yes	no	no	6.78 ± 0.29 [M]	DGC(2019)	2.04
NGC 1398	LTG	24.8	SBab	yes	yes	no	no	8.03 ± 0.11 [S]	DGC(2019)	2.29
NGC 2273 ^a	LTG	31.6	SBa	yes	yes	no	no	6.97 ± 0.09 [M]	DGC(2019)	2.15
NGC 2748 ^a	LTG	18.2	Sbc	no	yes	no	no	7.54 ± 0.21 [G]	DGC(2019)	1.98
NGC 2960 ^a	LTG	71.1	Sa (merger)	no	yes	no	no	7.06 ± 0.17 [M]	DGC(2019)	2.22 [11i]
NGC 2974	LTG	21.5	SB	yes	yes	no	yes	8.23 ± 0.07 [S]	DGC(2019)	2.37
NGC 3031	LTG	3.5	SABab	no	yes	no	no	7.83 ± 0.09 [G]	DGC(2019)	2.18
NGC 3079 ^a	LTG	16.5	SBcd	yes	yes	no	yes	6.38 ± 0.12 [M]	DGC(2019)	2.24
NGC 3227 ^a	LTG	21.1	SABa	yes	yes	no	yes	7.88 ± 0.14 [SG]	DGC(2019)	2.10
NGC 3368 ^a	LTG	10.7	SABa	yes	yes	no	no	6.89 ± 0.09 [SG]	DGC(2019)	2.07
NGC 3393 ^a	LTG	55.8	SBa	yes	yes	no	yes	7.49 ± 0.05 [M]	DGC(2019)	2.30
NGC 3627 ^a	LTG	10.6	SBb	yes	yes	no	yes	6.95 ± 0.05 [S]	DGC(2019)	2.10
NGC 4151	LTG	19.0	SABa	yes	yes	no	yes	7.68 ± 0.37 [SG]	DGC(2019)	1.96
NGC 4258	LTG	7.6	SABb	yes	yes	no	yes	7.60 ± 0.01 [M]	DGC(2019)	2.12
NGC 4303 ^a	LTG	12.3	SBbc	yes	yes	no	yes	6.58 ± 0.17 [G]	DGC(2019)	1.98
NGC 4388 ^a	LTG	17.8	SBcd	yes	yes	no	yes	6.90 ± 0.11 [M]	DGC(2019)	2.00
NGC 4395	LTG	4.8	SBm	yes	yes	no	yes	5.64 ± 0.17 [G]	DGC(2019)	1.42
NGC 4501 ^a	LTG	11.2	Sb	no	yes	no	yes	7.13 ± 0.08 [S]	DGC(2019)	2.22
NGC 4594	LTG	9.6	Sa	no	yes	no	yes	8.81 ± 0.03 [S]	DGC(2019)	2.35
NGC 4699 ^a	LTG	23.7	SABb	yes	yes	no	no	8.34 ± 0.10 [S]	DGC(2019)	2.28
NGC 4736 ^a	LTG	4.4	SABab	no	yes	no	yes	6.78 ± 0.10 [S]	DGC(2019)	2.03
NGC 4826 ^a	LTG	5.6	Sab	no	yes	no	yes	6.07 ± 0.15 [S]	DGC(2019)	1.99
NGC 4945 ^a	LTG	3.7	SABc	no	yes	no	yes	6.15 ± 0.30 [M]	DGC(2019)	2.07
NGC 5055 ^a	LTG	8.9	Sbc	no	yes	no	no	8.94 ± 0.10 [G]	DGC(2019)	2.00
NGC 5495 ^a	LTG	101.1	SBc	yes	yes	no	no	7.04 ± 0.08 [M]	DGC(2019)	2.22 [11g]
NGC 5765b ^a	LTG	133.9	SABb	yes	yes	no	no	7.72 ± 0.05 [M]	DGC(2019)	2.21 [11g]
NGC 6264 ^a	LTG	153.9	SBb	yes	yes	no	yes	7.51 ± 0.06 [M]	DGC(2019)	2.20 [11f]
NGC 6323 ^a	LTG	116.9	SBab	yes	yes	no	no	7.02 ± 0.14 [M]	DGC(2019)	2.20 [11f]
NGC 6926 ^a	LTG	86.6	SBc	yes	yes	no	yes	7.74 ± 0.50 [M]	DGC(2019)	...
NGC 7582 ^a	LTG	19.9	SBab	yes	yes	no	yes	7.67 ± 0.09 [G]	DGC(2019)	2.07
UGC 3789 ^a	LTG	49.6	SABa	yes	yes	no	no	7.06 ± 0.05 [M]	DGC(2019)	2.03 [11f]
UGC 6093 ^a	LTG	152.8	SBbc	yes	yes	no	no	7.41 ± 0.03 [M]	DGC(2019)	2.19 [11f]
NGC 0613 ^a	LTG	17.2	SB(rs)bc	yes	yes	no	no	7.57 ± 0.15 [G]	Co+14(2019)	2.09
NGC 1365 ^a	LTG	17.8	SB(s)b	yes	yes	no	yes	6.60 ± 0.30 [G]	Co+14(2019)	2.15
NGC 1566 ^a	LTG	7.2	SAB(s)bc	yes	yes	no	yes	6.83 ± 0.30 [G]	Co+14(2019)	1.99
NGC 1672 ^a	LTG	11.4	SB(s)b	yes	yes	no	yes	7.70 ± 0.10 [G]	Co+14(2019)	2.04
NGC 3504	LTG	13.6	SABab	yes	yes	no	yes	7.01 ± 0.07 [G]	Ngu+10(2019)	2.08

Table 1 *continued*

Table 1 (continued)

Galaxy	Type	Distance	Morph	Bar	Disk	Core	AGN	$\log(M_{BH}/M_{\odot})$	Source	$\log(\sigma/\text{km s}^{-1})$
(1)	(2)	(3)	(4)	(5)	(6)	(7)	(8)	(9)	(10)	(11)

NOTE—Column: (1) Galaxy name. (2) Galaxy type: early-type or late-type. (3) Distance to the galaxy. (4) Galaxy Morphology. (5) Presence of bar. (6) Presence of a rotating intermediate-scale (ES) or large-scale (S0/Sp) disk. (7) Presence of a depleted stellar core. (8) Presence of active galactic nucleus. (9) Directly measured black hole mass along with measurement method indicated by [P]= proper motion, [S]= stellar-dynamical modeling, [G]= gas dynamical modeling, [SG]= stellar and gas dynamical modeling, [M]= megamaser kinematics, and [DI]= direct imaging. (10) Catalog references, where the information for column (2) to column (9) comes from SG(2016)= Savorgnan et al. (2016), GCS(2016)= Graham et al. (2016a), G+7(2016)= Graham et al. (2016b), SGD(2019)= Sahu et al. (2019), No+7(2007)= (Nowak et al. 2007), Ngu+10(2018)= Nguyen et al. (2018), Th+6(2019)= Thater et al. (2019), Bo+7(2019)= Boizelle et al. (2019), Hu+4(2011)= Huré et al. (2011), Gu+6(2014)= Gültekin et al. (2014), DGC(2019)= Davis et al. (2019), Co+14(2019)= Combes et al. (2019), and Ngu+10(2019)= Nguyen et al. (2019). (11) Central velocity dispersion of galaxies mostly archived in HYPERLEDA (Paturel et al. 2003) unless otherwise specified: [11a]= Walsh et al. (2015); [11b]= Graham et al. (2016b), [11c]= Dalla Bontà et al. (2009); [11d]=Greene et al. (2010); [11e]=Thater et al. (2019); [11f]=Kormendy & Ho (2013); [11g]= Greene et al. (2016), [11h]= van den Bosch (2016); [11i]= Saglia et al. (2016). Bulge and galaxy stellar masses can also be found in Savorgnan & Graham (2016); Davis et al. (2019); and Sahu et al. (2019).

^a Alleged to host a pseudo-bulge according to Kormendy & Ho (2013), Saglia et al. (2016), and the references mentioned in Table 1 of Davis et al. (2017). NGC 0613, NGC 1365, NGC 1566, and NGC 1672 are claimed to have pseudo-bulges by Combes et al. (2019).

^b Latest black hole mass measurement from the Event Horizon Telescope Collaboration through direct imaging (Event Horizon Telescope Collaboration et al. 2019).

3. $M_{BH}-\sigma$ RELATIONS

In this work, we use both the BCES⁷ (Akritas & Bershady 1996) routine and the bisector line from the modified FITEXY (Press et al. 1992) routine (MPFITEXY, Tremaine et al. 2002; Novak et al. 2006; Bedregal et al. 2006; Williams et al. 2010; Markwardt 2012) to establish the $M-\sigma$ relations. Both the BCES and MPFITEXY regression routines take into account the measurement errors in the X and Y coordinates and allow for intrinsic scatter in the data.

The BCES routine directly provides the forward regression BCES(Y|X) line, the inverse regression BCES(X|Y) line, and the regression line which symmetrically bisects the two, i.e., BCES(BISECTOR)⁸. However, to obtain a symmetrical treatment (MPFITEXY(BISECTOR)) of the data with the MPFITEXY routine requires averaging the inclination of the best-fit lines obtained from the forward (MPFITEXY(Y|X)) and inverse (MPFITEXY(X|Y)) regressions as explained in Novak et al. (2006).

We prefer the symmetric (bisector) regressions obtained from both the routines because we do not know whether the central SMBH mass fundamentally governs the central velocity dispersion of a galaxy or vice-versa, or indirectly through a third parameter. A symmetrical

regression is also preferable for theoretical grounds, see Novak et al. (2006).

In our plots, we show the BCES(BISECTOR) regression line. These are also presented in Table 2. In addition, asymmetric BCES(Y|X) and BCES(X|Y) regression parameters are also provided in the Appendix (Table 3). We do not provide the MPFITEXY parameters for our relations as these were found to always be consistent with the parameters obtained from the BCES routine within the $\pm 1\sigma$ confidence limits.

3.1. Galaxy Exclusions

We identify and exclude the following eight galaxies which may bias the $M_{BH}-\sigma$ relation: NGC 404; NGC 5102; NGC 5206; NGC 7457; IC 1481; NGC 4395; NGC 5055; and NGC 6926; where the last three galaxies are LTGs.

NGC 404 is the only galaxy anchoring the intermediate black hole mass end ($\lesssim 10^5 M_{\odot}$) of the relation, as such it may bias the best-fit line. Additionally, as we will see, NGC 404, NGC 5102, and NGC 5206, for whom we obtained black hole masses from the same group (Nguyen et al. 2017, 2018), all seem to lie above the $M_{BH}-\sigma$ relation defined by the remaining galaxies. As we have only a four galaxies (NGC 404, NGC 5102, NGC 5206, and NGC 4395) with $M_{BH} \lesssim 10^6 M_{\odot}$ (as can be seen in Figure 1 and further in the left-hand panel of Figure 2), we do not include them in our primary regressions. As noted above, this also helps us detect possible departures at the low-mass end.

NGC 7457 has an unusually low-velocity dispersion, possibly because of a counter-rotating core (Molaeinezhad et al. 2019), which makes it fall beyond the $\pm 2\sigma$ scatter bounds of our single regression relation.

⁷ The BCES routine was used via the PYTHON module written by Rodrigo Nemmen (Nemmen et al. 2012), which is available at <https://github.com/rsnemmen/BCES>.

⁸ BCES(Y|X) minimizes the offsets in the Y-direction, and BCES(X|Y) minimizes, the offsets in the X-direction.

Similarly, NGC 4395 and NGC 5055 have lower velocity-dispersion values than expected from the $M_{BH}-\sigma$ relation defined by the bulk of the sample, which makes them stand out from the, soon to be seen, best-fit lines. These three (NGC 7457, NGC 4395, and NGC 5055) outlying galaxies significantly affect our best-fit lines; hence we exclude them from our regressions in order to obtain more stable relations reflective of the majority of the population.

For IC 1481 and NGC 6926, we do not have a reliable measurement of their central velocity dispersion. We have also provided regression parameters including all excluded galaxies (except IC 1481 and NGC 6926) in Table 4 of the Appendix to show how much these few galaxies bias our best-fit lines. Overall, we exclude a total of 8 galaxies, which leaves us with a reduced sample of 137 galaxies.

In our reduced sample, five galaxies (NGC 1316, NGC 2960, NGC 5128, NGC 5018, and NGC 1194) are mergers identified by Kormendy & Ho (2013, their section 6.4), Saglia et al. (2016), and Sahu et al. (2019, see the light profile of NGC 1194 and references). A merger designation refers to the stage when a galaxy is yet to reach a relaxed (stable) post merger configuration. Kormendy & Ho (2013) suggest excluding mergers from the black hole scaling relations as they may bias the results. However, given the small number of mergers in our sample, and given that they are not (significant) outliers in the $M_{BH}-\sigma$ relations, we include them.

Additionally, NGC 4342 (Blom et al. 2014) and NGC 4486B (Batcheldor et al. 2010) are tidally stripped of their stellar mass by the gravitational pull of their massive companion galaxies NGC 4365 and NGC 4486 (M87), respectively. However, stripping of the outer stellar mass should not considerably affect the central stellar velocity dispersions, hence we also include these galaxies in our $M_{BH}-\sigma$ relations. These seven (mergers and stripped) galaxies are displayed with a different color (yellow star) in our Figure 1, to show that these galaxies are neither significant outliers nor do they bias the relation. Excluding these mergers and stripped galaxies changes the slope and intercept of the best-fit lines on an average by 1% and 0.1%, respectively, which is insignificant compared to the error bars on the slopes and intercepts.

In what follows, we divided our reduced sample of 137 galaxies into various categories, for example, early-type and late-type galaxies, Sérsic and core-Sérsic galaxies, galaxies with and without a disk, galaxies with and without a bar, and galaxies with and without an AGN. The following subsections describe the scaling relations obtained for these sub-morphological classes.

3.2. Early-type Galaxies and Late-type Galaxies

After excluding the eight galaxies mentioned in Section 3.1, our reduced sample is comprised of 91 ETGs and 46 LTGs⁹. The BCES(BISECTOR) regression line for the ETGs can be expressed as,

$$\log(M_{BH}/M_{\odot}) = (5.71 \pm 0.33) \log\left(\frac{\sigma}{200 \text{ km s}^{-1}}\right) + (8.32 \pm 0.05), \quad (1)$$

with a total rms scatter of $\Delta_{rms|BH} = 0.44$ dex in the $\log M_{BH}$ -direction. The relation followed by the LTGs can be formulated as,

$$\log(M_{BH}/M_{\odot}) = (5.82 \pm 0.75) \log\left(\frac{\sigma}{200 \text{ km s}^{-1}}\right) + (8.17 \pm 0.14), \quad (2)$$

with $\Delta_{rms|BH} = 0.63$ dex. The slopes and intercepts of both lines (see Figure 1) are consistent within the $\pm 1\sigma$ confidence limits, suggesting a single M_{BH} versus σ relation for both ETGs and LTGs is adequate. Therefore, we perform a single regression on the total sample of 137 galaxies, which is represented in Figure 2. The BCES(BISECTOR) best-fit line obtained from the single regression can be written as

$$\log(M_{BH}/M_{\odot}) = (6.10 \pm 0.28) \log\left(\frac{\sigma}{200 \text{ km s}^{-1}}\right) + (8.27 \pm 0.04), \quad (3)$$

with $\Delta_{rms|BH} = 0.53$ dex. However, as we will see in the following subsection, it is deceptive to think that one line is sufficient to understand the connection between supermassive black holes and the stellar velocity dispersion of the host galaxies.

Although we assigned a 10% uncertainty to the measured velocity dispersions, as discussed in Section 2, we find consistent results for our regressions when using either 5% or 15% uncertainties on σ , or using the uncertainties provided in HYPERLEDA and the other corresponding sources (Column 11 of Table 1). In addition to the BCES(BISECTOR) regression line parameters, the slopes and intercepts of the best-fit lines from the BCES($M_{BH}|\sigma$) and BCES($\sigma|M_{BH}$) regressions, along with the scatter, Pearson correlation coefficient, and Spearman rank-order correlation coefficients are presented in Table 3 in the Appendix.

In the left hand panel of Figure 2, we show the galaxies NGC 404, NGC 5102, NGC 5206, and NGC 4395 which are excluded from our regressions because they are the only data points in the low-mass ($M_{BH} \lesssim$

⁹ As noted in Section 3.1, results including the six of these eight galaxies with velocity dispersions can be found in the Appendix.

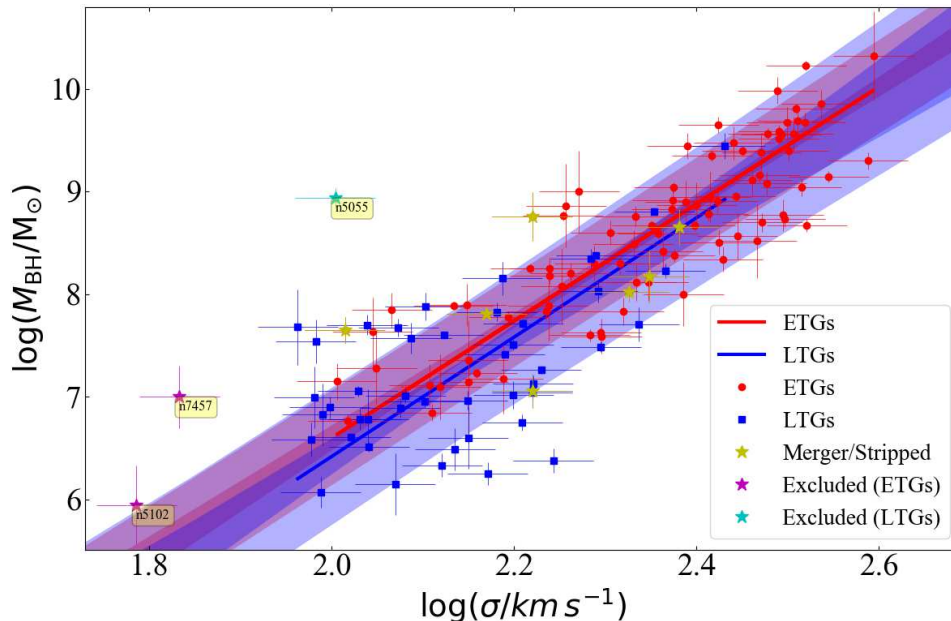


Figure 1. Black hole mass versus central velocity dispersion relation followed by 91 ETGs (red circles) and 46 LTGs (blue squares). Dark red and blue lines are the BCES(BISECTOR) best-fit lines for ETGs and LTGs. The red and blue bands around these lines represent the $\pm 1\sigma$ uncertainty limits in their slopes and the intercepts. Furthermore, the light red and light blue shaded regions depict the $\pm 1\sigma$ scatter in the ETG and LTG samples, respectively. The yellow stars represent either merger or stripped galaxies. Labeled data-points represent galaxies excluded from the regressions, as noted in the inset legend. The best-fit lines for the two sub-populations are consistent (Equations 1 and 2) with each other, suggesting a single $M_{BH}-\sigma$ relation as shown in Figure 2.

$10^6 M_{\odot}$) range. The first three galaxies are taken from Nguyen et al. (2017, 2018). These galaxies depart from the line defined by galaxies with $M_{BH} \gtrsim 10^6 M_{\odot}$, perhaps revealing here a bend in the $M_{BH}-\sigma$ relation not detected by Nguyen et al. (2017, 2018). Including these galaxies in the regression produces a shallower slope of 5.39 ± 0.34 (cf. 6.10 ± 0.28 from Equation 3), suggesting these four galaxies may have a significant effect on our best-fit line for the full sample, which is why we decided to exclude them from our regressions.

In the left-hand panel of Figure 2, we have additionally highlighted galaxies alleged to have pseudo-bulges by Kormendy & Ho (2013), Saglia et al. (2016), and a few additional studies mentioned in Davis et al. (2017, their Table 1). These pseudo-bulges appear to follow the $M_{BH}-\sigma$ relation (see Figure 2); they are distributed about the best-fit (green) line, though with slightly more scatter than that of galaxies hosting classical bulges. However, given the difficulties in assigning a bulge type (see Footnote 2), it is premature to draw conclusions about the co-evolution or not of black holes in pseudo-bulges.

In a recent work, van den Bosch (2016) fit a single $M_{BH}-\sigma$ line to all the morphological types of galaxies, and reported $M_{BH} \propto \sigma^{5.35 \pm 0.23}$, which is shallower than our relation (Equation 3). We suspect that their best-

fit line may be influenced by the inclusion of a few low-mass dwarf galaxies, the use of upper limits on M_{BH} for many galaxies, and 24 reverberation-mapped black hole mass estimates (pre-calibrated to a prior $M_{BH}-\sigma$ relation with a slope of 5.31 ± 0.33 from Woo et al. 2013).

3.3. Sérsic and Core-Sérsic Galaxies

Out of the 91 ETGs in our reduced sample, 35 are core-Sérsic, i.e., galaxies which have a deficit of stars at their center relative to the outer Sérsic profile (Graham et al. 2003), while the remaining 56 ETGs, and all 46 LTGs, are Sérsic galaxies. Core-Sérsic or Sérsic classifications for each of our galaxies are borrowed from their parent works, i.e., Savorgnan et al. (2016), Davis et al. (2019), and Sahu et al. (2019), as mentioned in Table 1 (Column 10).

We first performed separate regressions for the Sérsic and core-Sérsic ETGs, then on the combined sample of 137 galaxies. The $M_{BH}-\sigma$ plots for these two divisions are shown in Figure 3 and Figure 4, respectively.

Sérsic and core-Sérsic categorization reveals two different relations followed by the two sub-populations. The symmetric best-fit line followed by the early-type Sérsic

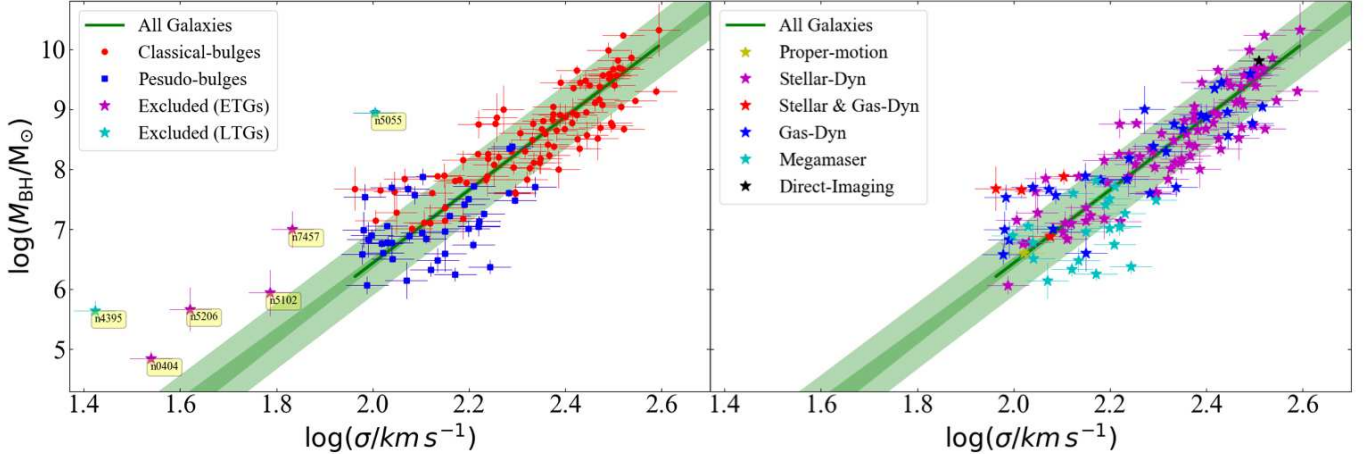


Figure 2. Black hole mass versus central velocity dispersion relation obtained from a single regression on the sample of 137 ETGs and LTGs. The dark green line is the best-fit BCES(BISECTOR) regression line (Equation 3). The dark green band around the dark green line shows the $\pm 1\sigma$ uncertainty in the slope and intercept of the best-fit line. The light green shaded region represents the $\pm 1\sigma$ scatter in the data. This explanation of the dark and light-shaded regions around the best-fit line applies to all the subsequent figures in this paper. Labeled data-points in the left-hand panel represent all the excluded galaxies except for IC 1481 and NGC 6926, which cannot be included as they have no reliable σ measurements (see Section 3.1). The blue squares in the left-hand panel represent the galaxies which are alleged to contain pseudobulges by Kormendy & Ho (2013), Saglia et al. (2016), and the references mentioned in Table 1 of Davis et al. (2017). This plot suggests that pseudobulges do follow the $M_{BH}-\sigma$ relation similar to classical bulges. Moreover, these pseudobulges are distributed above and below the best-fit line, albeit they are spread over a short range of M_{BH} and σ . Right-hand panel shows the same plot but each galaxy is color coded according to the method used to measure its black hole mass.

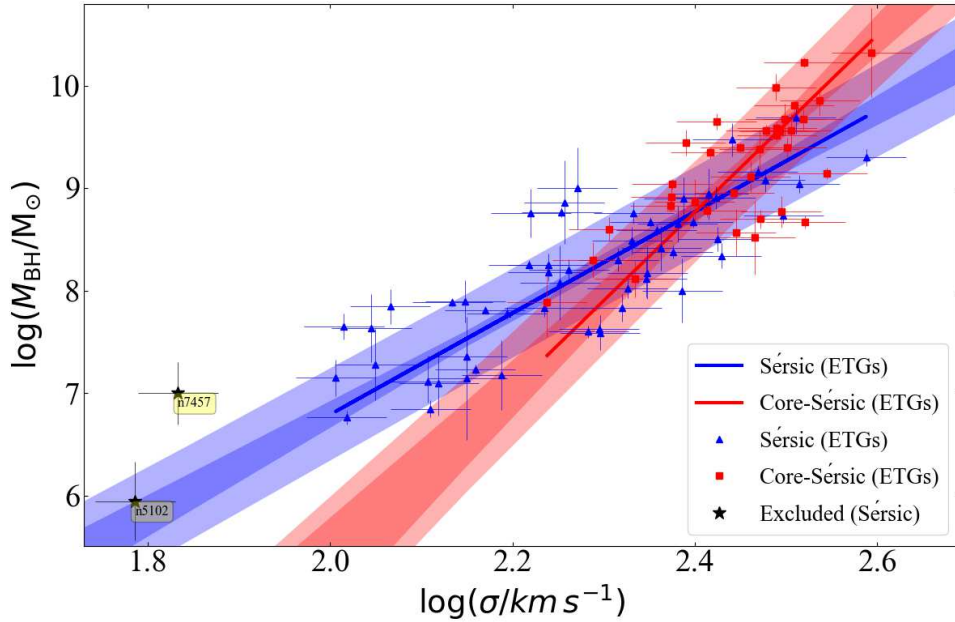


Figure 3. Black hole mass versus central velocity dispersion relation for Sérsic (blue triangles) and core-Sérsic (red squares) ETGs. These two sub-populations follow two distinct relations (Equations 4 and 6), suggesting a broken $M_{BH}-\sigma$ relation.

galaxies can be expressed as

$$\log(M_{BH}/M_{\odot}) = (4.95 \pm 0.38) \log\left(\frac{\sigma}{200 \text{ km s}^{-1}}\right) + (8.28 \pm 0.06), \quad (4)$$

with $\Delta_{rms|BH} = 0.42$ dex, represented by the dark blue line in Figure 3. The total Sérsic population, consisting of 102 early- and late-type Sérsic galaxies, produces the relation

$$\log(M_{BH}/M_{\odot}) = (5.75 \pm 0.34) \log\left(\frac{\sigma}{200 \text{ km s}^{-1}}\right) + (8.24 \pm 0.05), \quad (5)$$

represented by the dark blue line in Figure 4, with $\Delta_{rms|BH} = 0.55$ dex. The best-fit lines obtained for only early-type Sérsic galaxies and for all the Sérsic galaxies are marginally consistent with each other within the $\pm 1\sigma$ bound of their slopes and intercepts.

However, the core-Sérsic galaxies follow a much steeper $M_{BH}-\sigma$ relation, with $\Delta_{rms|BH} = 0.46$ dex, as is shown by the dark red lines in both Figures 3 and 4, which can be expressed as

$$\log(M_{BH}/M_{\odot}) = (8.64 \pm 1.10) \log\left(\frac{\sigma}{200 \text{ km s}^{-1}}\right) + (7.91 \pm 0.20). \quad (6)$$

The slope of this line is inconsistent with that of the Sérsic galaxies. The difference in their slopes reveals that Sérsic and core-Sérsic galaxies follow two distinct relations, potentially linked to the evolutionary paths followed by these two type of galaxies, i.e., evolution via major dry-mergers versus gas-rich mergers and accretion events. Additionally, core-Sérsic galaxies follow a steeper relation, that is, their σ values do not appear to saturate or asymptote at the high black hole mass end.

Core-Sérsic galaxies are old, gas-poor, massive galaxies, many of which are BCGs which have undergone multiple major (equal mass) dissipation-less dry-mergers. During a dry-merger, their central SMBHs inspiral, expelling out stars from the center, thereby creating a deficit of light at the core of the resulting galaxy. The stellar mass deficit, relative to the central black hole mass, may be a measure of the number of dry mergers a galaxy has undergone (Merritt & Milosavljević 2005; Savorgnan & Graham 2015), with the radial size of the depleted core known to be correlated with the black hole mass (Dullo & Graham 2014; Thomas et al. 2016; Mehrgan et al. 2019).

The steeper $M_{BH}-\sigma$ relation for core-Sérsic galaxies reveals that dry mergers do not increase the velocity dispersion, relative to the increased black hole mass, at the pace followed by Sérsic galaxies (built through either gas-rich mergers or accretion of gas

from their surroundings). This has also been suggested by some theoretical studies (e.g., Ciotti & van Albada 2001; Oser et al. 2012; Shankar et al. 2013; Hilz et al. 2013). Furthermore, Volonteri & Ciotti (2013) used their analytical and semi-analytical models to show that simulated BCGs are offset from the $M_{BH}-\sigma$ relation defined by non-BCGs because they undergo multiple gas-poor (dry) mergers resulting in over-massive black holes with only mildly increased velocity dispersion.

3.4. Galaxies With a Disk (ES/S0/Sp) and Without a Disk (E)

ETGs include elliptical (E), elliptical (ES), and lenticular (S0) galaxies. Elliptical galaxies are pressure-supported, spheroid-dominated galaxies with minimal rotation. Elliptical galaxies host an intermediate-scale (rotating) stellar disk within their spheroids (Liller 1966; Graham et al. 2016a), while lenticular galaxies have a large-scale disk extending beyond their bulges (see Graham 2019a, for a detailed morphological classification grid). LTGs are spiral (Sp) galaxies with a bulge, a large-scale disk, and spiral arms. The LTGs in our sample are predominantly early-type spirals (Sa-Sb).

Our reduced sample of 137 galaxies is comprised of 44 elliptical galaxies which do not have a rotating disk, plus 93 galaxies with a disk, which includes 47 ES or S0-types (ETGs) and 46 spirals (LTGs).

We first performed separate regressions on the ETGs with (ES/S0) and without (E) a disk, as shown in Figure 5 where the blue and red lines correspond to $M_{BH} \propto \sigma^{4.93 \pm 0.39}$ and $M_{BH} \propto \sigma^{6.69 \pm 0.59}$, respectively. Then we performed regressions on all types of galaxies with a disk (ES/S0/Sp), and without a disk (E-types), as represented in Figure 6 where the blue lines define $M_{BH} \propto \sigma^{5.72 \pm 0.34}$ and the red line is the same as that in Figure 5, i.e., $M_{BH} \propto \sigma^{6.69 \pm 0.59}$. Full equations of the best-fit lines can be found in our Table 2.

Not surprisingly, we find that galaxies with and without a disk seem to follow two slightly different relations in both cases (ETG-only, ETG+LTG). This is more apparent for the ETG sample (Figure 5) than for the total sample (Figure 6) because upon including spiral galaxies with ETGs with a disk (ES/S0), the apparent difference in slopes of the blue and red lines reduces.

This difference in the $M_{BH}-\sigma$ relations due to galaxies with and without a disk is likely because most of the elliptical galaxies in our sample are (massive) core-Sérsic galaxies and almost all the galaxies with a rotating disk are Sérsic galaxies. The extent of the difference between the $M_{BH}-\sigma$ relation for core-Sérsic and Sérsic galaxies is greater than that of the relations followed by the galaxies with and without a disk. This suggests that the two

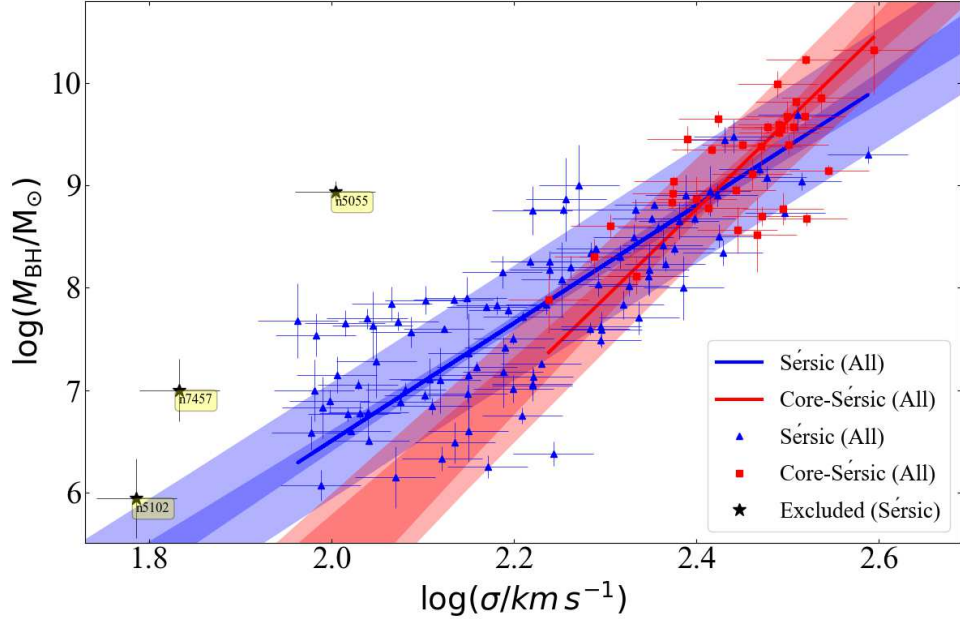


Figure 4. Similar to Figure 3, but including all early- and late-type Sérsic galaxies in the same category (blue triangles) while all core-Sérsic galaxies (red squares) are early-type galaxies. Upon including the LTGs (spirals) which are all Sérsic galaxies, we still find two different $M_{BH}-\sigma$ relations followed by the Sérsic and core-Sérsic galaxies (Equations 5 and 6).

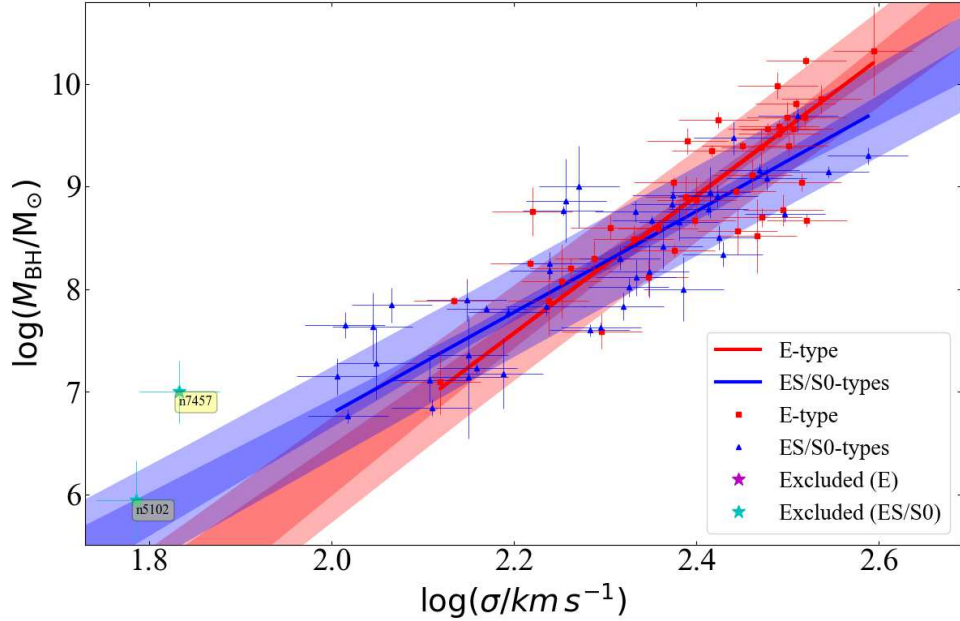


Figure 5. Black hole mass versus central velocity dispersion relations for ETGs with a disk (ES/S0-types) and ETGs without a disk (E-type). We find two slightly different relations for galaxies with and without a disk, which is similar (but less pronounced) to the separation in the $M_{BH}-\sigma$ diagram due to Sérsic and core-Sérsic galaxies (see Figure 3). This is not surprising as most of the elliptical galaxies in our sample are core-Sérsic galaxies and most of the ETGs with a disk (ES/S0-types) are Sérsic galaxies, hence the difference is caused by core-Sérsic and Sérsic galaxies.

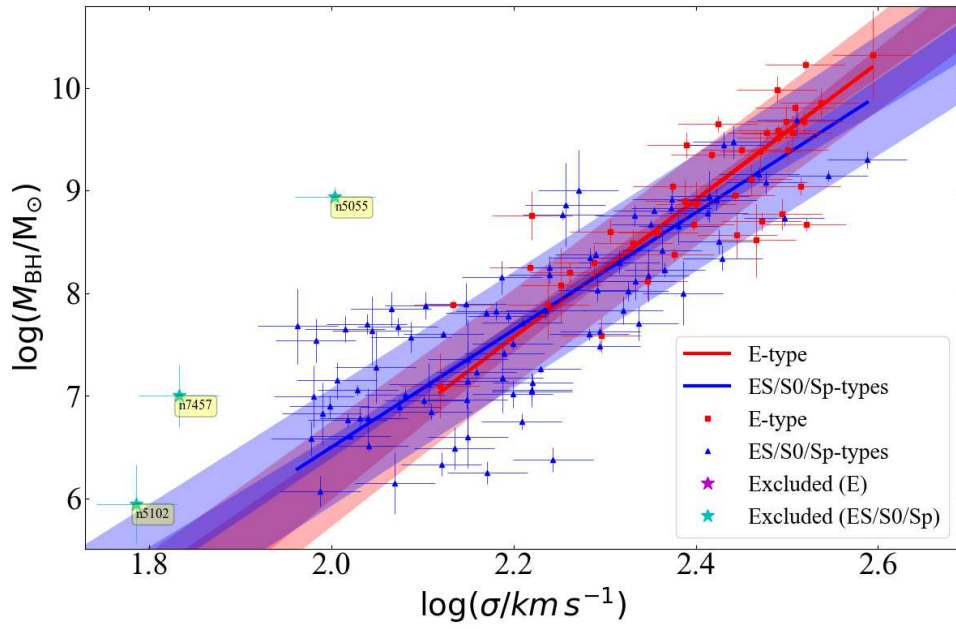


Figure 6. Similar to Figure 5, but now including spiral (Sp) galaxies—all of which have an extended rotating disk—along with the elliptical (ES) and lenticular (S0) galaxies in the category of galaxies with a disk, while elliptical (E) galaxies without a disk are all ETGs. Here, we again find two slightly different relations in the M_{BH} - σ diagram, but not as pronounced as between Sérsic and core-Sérsic galaxies. See Table 2 for full equations of the two lines.

distinct relations in the $M_{BH}-\sigma$ diagram are predominantly caused by core-Sérsic versus Sérsic galaxies. It should be noted that core-Sérsic galaxies can also have disks (e.g. [Dullo & Graham 2013, 2014; Dullo 2014](#)), for example the lenticular galaxies NGC 524, NGC 584, NGC 3706, NGC 4751, and NGC 5813 in our sample have depleted stellar cores.

We speculate that [Savorgnan & Graham \(2015\)](#) failed to detect different $M_{BH}-\sigma$ relations for core-Sérsic and Sérsic galaxies, or slow and fast rotators¹⁰, because of their smaller sample size. However, some of their core-Sérsic galaxies can be spotted to be offset from their single $M_{BH}-\sigma$ relation at the high-mass end.

3.5. Barred and Non-barred Galaxies

In the past, some observational studies ([Graham 2007; Hu 2008; Graham 2008a,b](#)) and simulations ([Brown et al. 2013; Hartmann et al. 2014](#)) have revealed that barred galaxies are offset towards the higher σ side in the $M_{BH}-\sigma$ diagram. Based on that offset, these studies suggest that barred galaxies should be separated from non-barred galaxies in order to obtain $M_{BH}-\sigma$ relations for barred and non-barred galaxies.

To investigate the above offset using our larger dataset, accompanied with our revised classifications based upon multi-component decompositions, we also divided our sample into barred and non-barred galaxies, and performed separate regressions on both populations. This was first done for barred and non-barred ETGs, then using the total (reduced) sample of 136 galaxies, as shown in Figures 7 and 8, respectively. Our ETG sample consists of 17 barred and 73 non-barred galaxies, while the full sample comprises 50 barred and 86 non-barred galaxies.

Surprisingly, we do not find any offset between barred and non-barred galaxies, in either case, i.e., only ETGs and the ETG + LTG sample. The best-fit line for the 17 barred ETGs is

$$\log(M_{BH}/M_{\odot}) = (5.98 \pm 0.80) \log\left(\frac{\sigma}{200 \text{ km s}^{-1}}\right) + (8.19 \pm 0.14), \quad (7)$$

with $\Delta_{rms|BH} = 0.41$ dex. However, we require a larger sample of barred ETGs for a robust relation. The 74 non-barred ETGs define the following relation, with $\Delta_{rms|BH} = 0.43$,

$$\log(M_{BH}/M_{\odot}) = (5.35 \pm 0.39) \log\left(\frac{\sigma}{200 \text{ km s}^{-1}}\right) + (8.37 \pm 0.06). \quad (8)$$

¹⁰ Note: ES galaxies are both fast rotators and slow rotators (e.g., [Bellstedt et al. 2017](#)).

The 50 barred ETG + LTG population defines the line,

$$\log(M_{BH}/M_{\odot}) = (5.30 \pm 0.54) \log\left(\frac{\sigma}{200 \text{ km s}^{-1}}\right) + (8.14 \pm 0.10), \quad (9)$$

with $\Delta_{rms|BH} = 0.45$ dex. The 87 non-barred galaxies define the relation

$$\log(M_{BH}/M_{\odot}) = (6.16 \pm 0.42) \log\left(\frac{\sigma}{200 \text{ km s}^{-1}}\right) + (8.28 \pm 0.06), \quad (10)$$

with $\Delta_{rms|BH} = 0.51$ dex. The best-fit lines for the barred and non-barred galaxies are consistent within the $\pm 1\sigma$ bounds of their slopes and intercepts, suggesting no significant offset between barred and non-barred galaxies.

3.5.1. Investigating Previous Offsets

To find the reason behind the offset observed by [Graham & Scott \(2013\)](#), we have compared their regression lines with ours obtained using the latest M_{BH} , σ , and updated bar-morphologies. Their sample of 72 galaxies was comprised of 21 barred and 51 non-barred galaxies, according to the morphological classifications they adopted, which were obtained from the NASA/IPAC Extragalactic Database (NED). All of their galaxies are present in our current sample, and in order to make a comparison, we use only the galaxies present in the data-set of [Graham & Scott \(2013\)](#).

Interestingly, out of those common 72 galaxies, we have classified 27 as barred, and 45 as non-barred. The barred and non-barred classifications for our current sample are based on the morphologies obtained from the multi-component decompositions of these galaxies presented in our recent works ([Savorgnan & Graham 2016; Davis et al. 2019; Sahu et al. 2019](#)). We notice that in the data-set of [Graham & Scott \(2013\)](#), seven barred galaxies (NGC 224, NGC 2974, NGC 3245, NGC 3998, NGC 4026, NGC 4388, and NGC 6264) were misclassified as non-barred due to the presence of weak bars not detected in optical images ([Eskridge et al. 2000](#))¹¹. Also, one non-barred galaxy (NGC 4945) in their sample appears to have been misclassified as barred, with [Davis et al. \(2019\)](#) reporting only a nuclear bar too weak to include in their modelling.

The green and yellow lines in Figure 9 are the BCES symmetric best-fit lines from [Graham & Scott \(2013\)](#) for

¹¹ [Eskridge et al. \(2000\)](#) claim that bars are more detectable in NIR band than optical. However, see [Buta et al. \(2010, and references therein\)](#) which suggest that bar-fraction is similar in the two wavelengths.

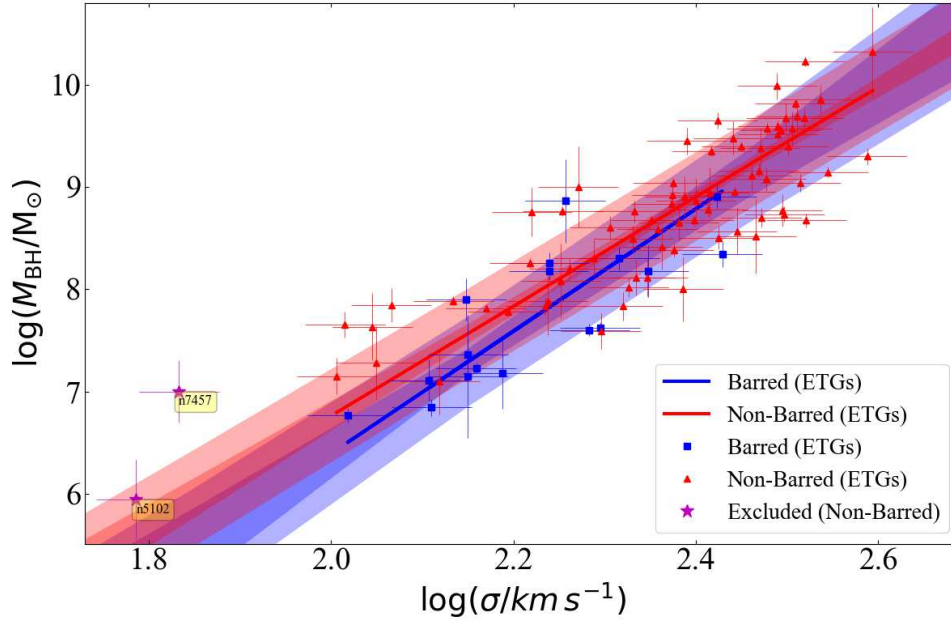


Figure 7. Black hole mass versus central velocity dispersion relation for barred and non-barred ETGs. Although we only have a small sample of 17 barred ETGs, the consistency of the two regression lines (blue and red lines) suggests no offset between barred (Equation 7) and non-barred (Equation 8) ETGs in the M_{BH} - σ diagram.

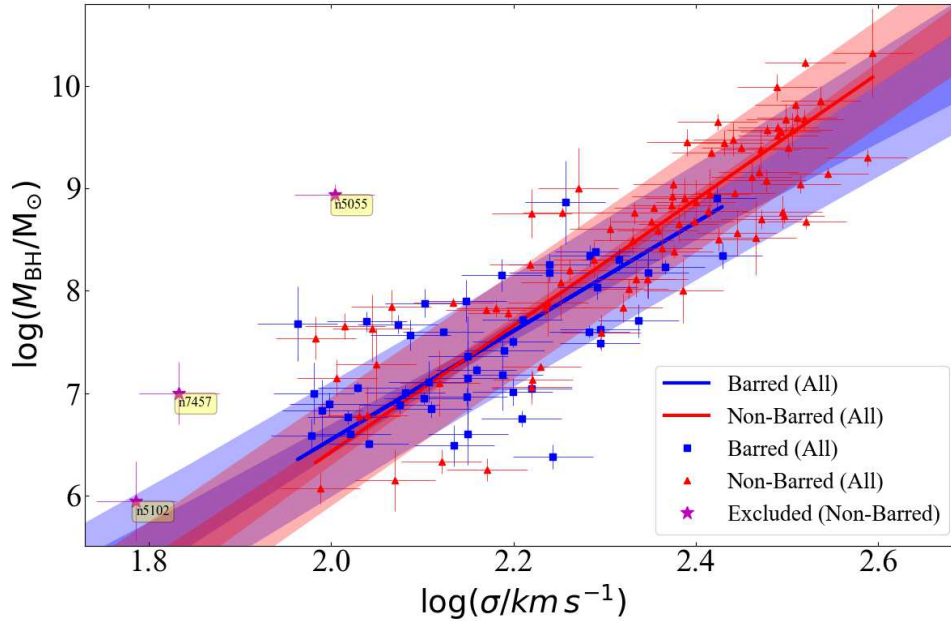


Figure 8. Similar to Figure 7, but including barred and non-barred late-type galaxies as well. The regression lines obtained for the 50 barred (blue line, Equation 9) and 87 non-barred (red line, Equation 10) galaxies are overlapping and consistent with each other, implying no-offset between barred and non-barred galaxies.

the barred and non-barred galaxies, respectively. These two lines are offset by ~ 0.5 dex at the median velocity dispersion of 200 km s^{-1} . The blue and red BCES bisector lines for the 72 reclassified barred and non-barred galaxies from our current data-set, are offset by only 0.16 dex. Moreover, on using the total (reduced) sample of 137 galaxies comprising 50 barred and 87 non-barred galaxies, as is represented in Figure 8, the offset reduces to 0.14 dex (see Equations 9 and 10).

We find that there are two main reasons why [Graham & Scott \(2013\)](#) found an offset. First, they largely classified their galaxies as barred or non-barred based on the morphologies provided by NED, which are mainly from the RC3 catalog ([de Vaucouleurs et al. 1991](#)) and in many cases it failed to identify bars and some other galaxy structures as well. The second reason is that their sample of 72 galaxies lacked (a sufficiently large sample of) barred galaxies residing above their regression line (the green line in Figure 9). Another reason for the difference might have been the updated black hole masses and velocity dispersions. For example, the updated ([Greene & Ho 2006](#)) velocity dispersion for the barred spiral galaxy NGC 4151 is $91.8 \pm 9.9 \text{ km s}^{-1}$, which is notably different from the old value of $156 \pm 7.8 \text{ km s}^{-1}$ reported in HYPERLEDA. However, we have found that, collectively, the updated velocity dispersions do not seem to have a significant effect on the offset between the regression lines for the barred and non-barred galaxies, because the latest σ values are not particularly different for most of the galaxies.

3.5.2. Strong versus Weak or Faint Bars

We also investigated if weak/faint barred galaxies are biasing our barred $M_{BH}-\sigma$ relation (Equation 9). There was a possibility that perhaps most of the weak/faint barred galaxies fall above the best-fit relation (blue line in Figure 8) for the barred galaxies in our current sample, and thereby reduce the offset between the best-fit relation for barred and non-barred galaxies.

For this investigation, we used the bar-to-total (galaxy) luminosity (L_{bar}/L_{tot}) ratio to categorize our barred galaxies into strong and weak/faint categories. However, as we were not sure of where to make the cut, we performed this test twice, first making the division at $L_{bar}/L_{tot} = 0.05$, then at $L_{bar}/L_{tot} = 0.1$. Figure 10 shows the barred galaxies color coded as black strong-barred ($L_{bar}/L_{tot} \geq 0.1$), yellow faint-barred ($L_{bar}/L_{tot} \leq 0.05$), and green with intermediate bar strength ($0.05 < L_{bar}/L_{tot} < 0.1$). For 14 barred-galaxies, 9 of which are from ([Savorgnan & Graham 2016](#)), 4 are from [Combes et al. \(2019\)](#), and one is from [Nguyen et al. \(2019\)](#), we do not have the luminosity of

the bar. Hence, we categorized them on the basis of their multi-component decomposition profile, the morphological bar classification provided by the literature, and a visual inspection of their images which was also performed for all the other barred galaxies. Overall, our total sample of 50 barred galaxies consists of 27 strong, 10 weak/faint, and 13 intermediate-strength barred galaxies.

For the first test, i.e., for the division at $L_{bar}/L_{tot} = 0.05$, all the strong (and intermediate) barred galaxies are distributed almost uniformly about the best-fit (blue) line for the barred galaxies, and many of the faint barred galaxies are below the best-fit line (see Figure 10). This suggests that galaxies with faint-bars do not minimize the offset between barred and non-barred galaxies. As for the second cut at $L_{bar}/L_{tot} = 0.1$, we can see in Figure 10, that most of the intermediate and faint barred galaxies are below the best-fit line for barred-galaxies, again indicating that weak/faint-barred, or even intermediate-barred galaxies, do not take part in reducing the offset between barred and non-barred galaxies. Strongly-barred galaxies are distributed above and below the best-fit line for barred galaxies.

3.6. Galaxies with and without an AGN

Our reduced sample of 137 galaxies includes 41 galaxies hosting an AGN. We identified the AGN hosts using the 13th edition of the catalog of quasars and active nuclei presented by [Véron-Cetty & Véron \(2010\)](#). Interestingly, these AGN hosts are spread almost uniformly about the best-fit bisector regression line (for the sample of 137 galaxies) for the range of M_{BH} and σ that we have, indicating that galaxies with and without an AGN follow a single relation.

Also, upon performing separate regressions on AGN hosts and galaxies without AGN, we obtain almost overlapping regression lines for the two categories, such that their slopes and intercept are consistent with each other within the $\pm 1\sigma$ confidence bounds (Figure 11). The regression parameters for the best-fit lines for galaxies with and without AGNs are given in Table 2. A galaxy hosting an AGN can be Sérsic or core-Sérsic, as can a galaxy without an AGN; hence, regardless of whether a galaxy hosts an AGN or not, the $M_{BH}-\sigma$ relations defined by Sérsic and core-Sérsic galaxies remain applicable, and should be used depending on the presence or absence of a core (deficit of star light, not due to dust obscuration).

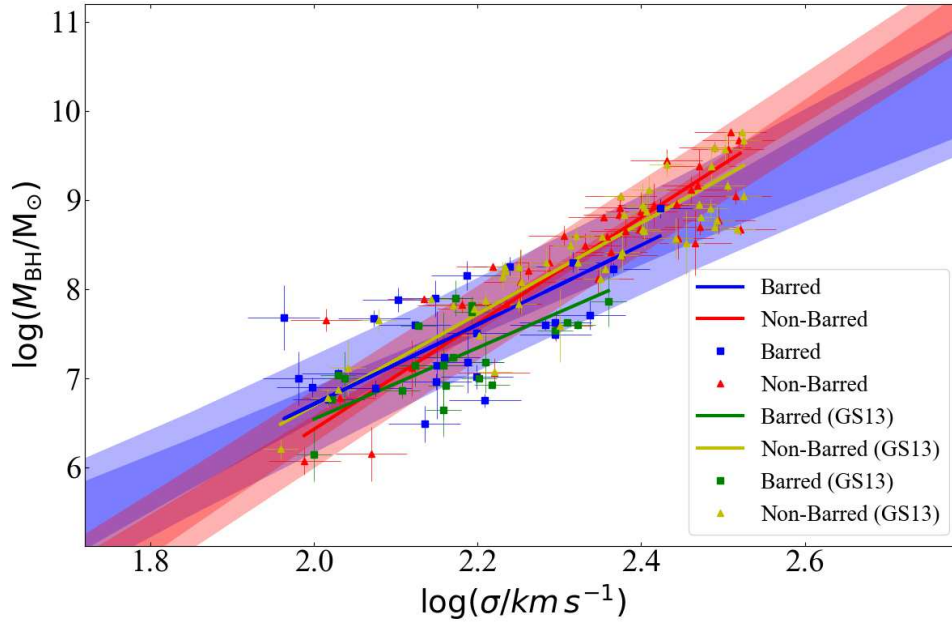


Figure 9. Comparison of our M_{BH} - σ relations for barred and non-barred galaxies with the relations reported in [Graham & Scott \(2013, GS13\)](#). Their galaxy sample is a sub-set of our current sample, thus, for a comparison, we use our latest data for the galaxies in their sample, applied with our new bar morphologies (blue and red points). The barred and non-barred data points (i.e., the green squares and yellow triangles, respectively) of [Graham & Scott \(2013\)](#) represent the M_{BH} , σ , and bar classifications they used. Using the same galaxy sample as that of [Graham & Scott \(2013\)](#), we do not find any significant offset between barred and non-barred galaxies.

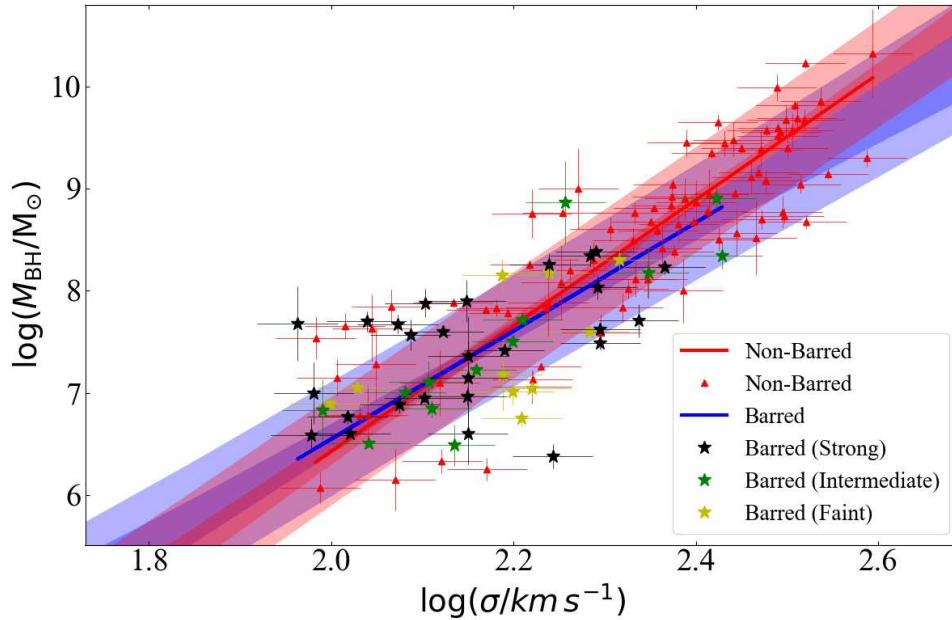


Figure 10. Similar to Figure 8, but now categorizing our barred galaxies into strong, intermediate, and faint barred galaxies.

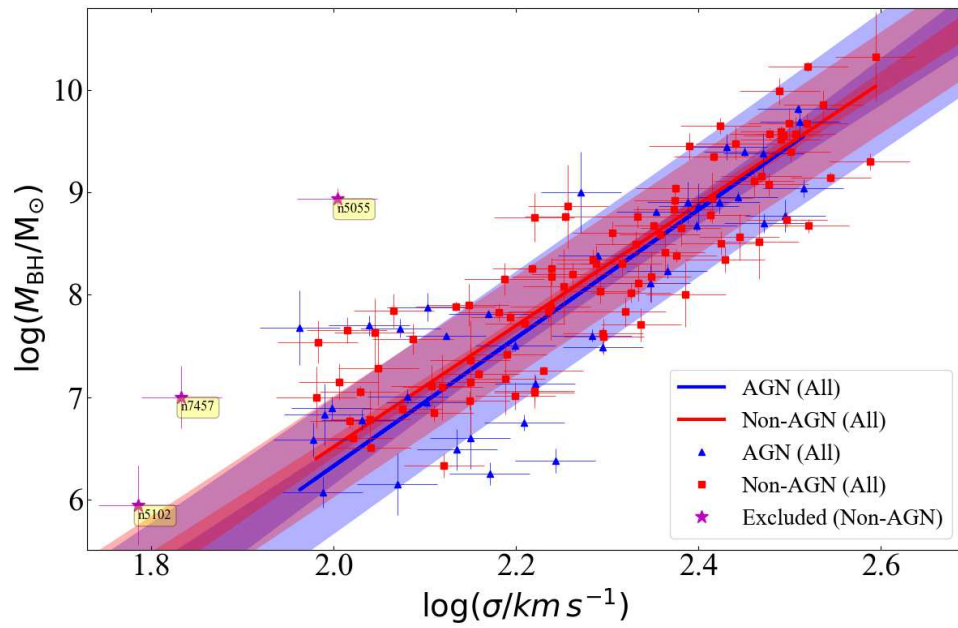


Figure 11. Black hole mass versus velocity dispersion followed by galaxies hosting an AGN and galaxies without an AGN.

Table 2. Linear Regressions [$\log(M_{\text{BH}}/M_{\odot}) = \alpha \log(\sigma/200) + \beta$]

Category	Number	α	β	ϵ	$\Delta_{r_{\text{rms}} _{\text{BH}}}$	r	r_s
(1)	(2)	(3)	(dex)	(dex)	(dex)	(7)	(8)
Early-Type Galaxies	91	5.71 ± 0.33	8.32 ± 0.05	0.32	0.44	0.86	0.85
Late-Type Galaxies	46	5.82 ± 0.75	8.17 ± 0.14	0.57	0.63	0.59	0.49
All Galaxies	137	6.10 ± 0.28	8.27 ± 0.04	0.43	0.53	0.86	0.87
Sérsic Galaxies	102	5.75 ± 0.34	8.24 ± 0.05	0.46	0.55	0.78	0.78
Core-Sérsic Galaxies	35	8.64 ± 1.10	7.91 ± 0.20	0.25	0.46	0.73	0.65
Galaxies with a disk (ES, S0, Sp-types)	93	5.72 ± 0.34	8.22 ± 0.06	0.47	0.56	0.79	0.78
Galaxies without a disk (E-type)	44	6.69 ± 0.59	8.25 ± 0.10	0.30	0.43	0.82	0.80
Barred Galaxies	50	5.30 ± 0.54	8.14 ± 0.10	0.45	0.53	0.65	0.61
Non-Barred Galaxies	87	6.16 ± 0.42	8.28 ± 0.06	0.40	0.51	0.86	0.86
AGN host Galaxies	41	6.26 ± 0.49	8.21 ± 0.09	0.55	0.63	0.83	0.79
Galaxies without AGN	96	5.92 ± 0.31	8.30 ± 0.05	0.37	0.48	0.87	0.88

NOTE— Columns: (1) Subclass of galaxies. (2) Number of galaxies in a subclass. (3) Slope of the line obtained from the BCES(BISECTOR) regression. (4) Intercept of the line line obtained from the BCES(BISECTOR) regression. (5) Intrinsic scatter in the $\log M_{\text{BH}}$ -direction (using Equation 1 from Graham & Driver 2007). (6) Total root mean square (rms) scatter in the $\log M_{\text{BH}}$ direction. (7) Pearson correlation coefficient. (8) Spearman rank-order correlation coefficient.

4. INTERNAL CONSISTENCY BETWEEN THE $M_{\text{BH}}-M_{*,\text{GAL}}$, $M_{\text{BH}}-M_{*,\text{SPH}}$, AND $M_{\text{BH}}-\sigma$ RELATIONS

Recent studies by Sahu et al. (2019) and Davis et al. (2019) established robust $M_{\text{BH}}-M_{*,\text{gal}}$ and $M_{\text{BH}}-M_{*,\text{sph}}$ correlations for ETGs and LTGs, using a (reduced) sample of 76 ETGs and 40 LTGs, respectively. As elaborated above in Section 3, we also observe a strong correlation between black hole mass and the central stellar velocity dispersion, along with the discovery of two distinct relations in the $M_{\text{BH}}-\sigma$ diagram due to Sérsic and core-Sérsic galaxies.

The $M_{\text{BH}}-M_{*,\text{gal}}$ (and $M_{\text{BH}}-M_{*,\text{sph}}$) relations combined with our $M_{\text{BH}}-\sigma$ relations can predict the $M_{*,\text{gal}}-\sigma$ and $M_{*,\text{sph}}-\sigma$ relations. They should be compared with the observed $M_{*,\text{gal}}-\sigma$ and $M_{*,\text{sph}}-\sigma$ relations to check for internal consistency of our relations. The ETGs and LTGs of Sahu et al. (2019) and Davis et al. (2019), respectively, constitute 85% of the sample used in this work to obtain the $M_{\text{BH}}-\sigma$ relations, hence their $M_{\text{BH}}-M_{*,\text{gal}}$ and $M_{\text{BH}}-M_{*,\text{sph}}$ relations are appropriate for internal consistency checks. To derive the $\sigma-M_{*,\text{gal}}$ and $\sigma-M_{*,\text{sph}}$ relations, we used the galaxy and spheroid stellar masses measured in Davis et al. (2018), Davis et al. (2019) and Sahu et al. (2019).

Sérsic and core-Sérsic ETGs have been found to follow the same $M_{\text{BH}}-M_{*,\text{gal}}$ and $M_{\text{BH}}-M_{*,\text{sph}}$ relations in Sahu et al. (2019), such that $M_{\text{BH}} \propto M_{*,\text{gal}}^{1.65 \pm 0.11}$ and

$M_{\text{BH}} \propto M_{*,\text{sph}}^{1.27 \pm 0.07}$ for all ETGs, i.e., when combining those with a disk and those without a disk. Whereas, the LTGs in Davis et al. (2019), all of which are Sérsic galaxies, define the relations $M_{\text{BH}} \propto M_{*,\text{gal}}^{3.05 \pm 0.70}$ and $M_{\text{BH}} \propto M_{*,\text{sph}}^{2.16 \pm 0.32}$, with slopes almost twice that of the (single regression) slopes for ETGs in Sahu et al. (2019, see their Figure 11). However, separating the ETGs into those with and without a disk reveals that they follow two different $M_{\text{BH}}-M_{*,\text{sph}}$ relations with slopes of approximately 1.9 ± 0.2 but with intercepts offset by more than a factor of 10 in the M_{BH} -direction (Sahu et al. 2019, their Figure 8). While in the $M_{\text{BH}}-M_{*,\text{gal}}$ diagram, the two relations for ETGs with and without a disk agree with each other much more closely, suggesting that the $M_{\text{BH}}-M_{*,\text{gal}}$ relation obtained from the single regression is a reasonable approximation for ETGs with and without a disk. In the $M_{\text{BH}}-\sigma$ diagram, Sérsic and core-Sérsic galaxies in our total (ETG+LTG) sample define two distinct relations, see Equations 5 and 6, respectively.

Theoretically, to check on the consistency between all of these $M_{\text{BH}}-M_{*,\text{sph}}$, $M_{\text{BH}}-\sigma$, and $M_{*,\text{sph}}-\sigma$ relations for ETGs, we should use the two distinct $M_{\text{BH}}-M_{*,\text{sph}}$ relations for ETGs with and without a disk with the two $M_{\text{BH}}-\sigma$ relations for core-Sérsic and Sérsic ETGs (Section 3.3), to predict different $M_{*,\text{sph}}-\sigma$ relations for core-Sérsic ETGs with and without a disk and Sérsic ETGs with and without a disk. However, if we separate

the core-Sérsic (or Sérsic) ETGs into galaxies with and without a disk, each sub-population will be too small to derive a robust $M_{*,sph}-\sigma$ relation for comparison with the predicted relation. Hence, for the current consistency checks, we have used the following single regression relation for ETGs: $M_{BH}-M_{*,sph}^{1.27\pm 0.07}$.

Using $M_{BH} \propto \sigma^{8.64\pm 1.10}$ (Equation 6) for our core-Sérsic galaxies, all of which are ETGs, and the $M_{BH}-M_{*,gal}$ (and $M_{BH}-M_{*,sph}$) relations for the ETGs from Sahu et al. (2019), we expect the relations $M_{*,gal} \propto \sigma^{5.24\pm 0.75}$ and $M_{*,sph} \propto \sigma^{6.80\pm 0.94}$ for core-Sérsic galaxies. These two relations are found to be consistent with the directly derived relations $M_{*,gal} \propto \sigma^{6.07\pm 1.04}$ and $M_{*,sph} \propto \sigma^{6.41\pm 1.31}$, obtained for our core-Sérsic galaxies using the BCES(BISECTOR) regression.

Using the single relation for all (ETG+LTG) Sérsic galaxies, $M_{BH} \propto \sigma^{5.75\pm 0.34}$ (Equation 5), and the $M_{BH}-M_{*,gal}$ (and $M_{BH}-M_{*,sph}$) relations for the ETGs from Sahu et al. (2019), Sérsic ETGs are expected to follow $M_{*,gal} \propto \sigma^{3.48\pm 0.31}$ and $M_{*,sph} \propto \sigma^{4.52\pm 0.36}$. These are consistent with the directly-derived relations $M_{*,gal} \propto \sigma^{2.90\pm 0.36}$ and $M_{*,sph} \propto \sigma^{3.85\pm 0.46}$ using the BCES(BISECTOR) regression.

Similarly, for Sérsic LTGs, using our Equation 5 and the $M_{BH}-M_{*,gal}$ (and $M_{BH}-M_{*,sph}$) relations for LTGs from Davis et al. (2019), we predict the relations $M_{*,gal} \propto \sigma^{1.88\pm 0.45}$ and $M_{*,sph} \propto \sigma^{2.66\pm 0.42}$, which are consistent with the directly-derived relations $M_{*,gal} \propto \sigma^{2.00\pm 0.38}$ and $M_{*,sph} \propto \sigma^{2.96\pm 0.55}$. In the same way, the relations for all the other subcategories, as described in the above subsections, have been found to be internally consistent. In the following sections, we turn our attention to matters of external consistency.

5. THE $L-\sigma$ DIAGRAM

For half a century, astronomers have been studying the correlation between the luminosity of a galaxy and the velocity dispersion of the stars in it (Minkowski 1962). However, with the increase in the number of reliable measurements at high and low luminosities, various studies found different relations when using different samples (Faber & Jackson 1976; Schechter 1980; Malumuth & Kirshner 1981; Tonry 1981; Binney 1982; Farouki et al. 1983; Davies et al. 1983; Held et al. 1992; de Rijcke et al. 2005; Matković & Guzmán 2005; Lauer et al. 2007), which collectively suggested a broken or curved $L-\sigma$ relation (see Graham 2016; Graham & Soria 2019, for a brief overview of previous studies). Here, we re-investigate the bend or curve in the $L-\sigma$ diagram.

5.1. V -band Data-set

Using elliptical galaxies from the V-band dataset of Lauer et al. (2007), with several modifications, Kormendy & Bender (2013) reported a steep $L_V \propto \sigma^8$ relation for the core (core-Sérsic) elliptical galaxies, and $L_V \propto \sigma^4$ for the core-less (Sérsic) elliptical galaxies. Although they specifically mention the use of a symmetric least squares regression routine from Tremaine et al. (2002, modified FITEXY), the slopes they report seem to be obtained from an asymmetric regression, i.e., a least squares minimization of the offsets in the σ -direction over \mathfrak{M}_V which produces a steep $L_V-\sigma$ slope. The modified FITEXY routine from (Tremaine et al. 2002) does not directly provide a symmetric regression line: one first needs to obtain the forward ($Y|X$) and inverse ($X|Y$) regression lines using this routine, and then find the bisector line. For the data used by Kormendy & Bender (2013), we report here that the symmetric application of the modified FITEXY regression routine gives $L_V \propto \sigma^{4.39\pm 0.61}$ for the core-Sérsic elliptical galaxies, and $L_V \propto \sigma^{2.98\pm 0.31}$ for the Sérsic elliptical galaxies.

We have used all of the 178 ETGs (for which σ is available) from Lauer et al. (2007) to revisit the V-band $\mathfrak{M}_V-\sigma$ relations¹², except for the stripped M32-type¹³ compact elliptical galaxies which can bias the relation (Graham & Soria 2019, see their Figure 11). We updated the core designation for the galaxies NGC 4458, NGC 4473, NGC 4478, and NGC 4482 according to Kormendy et al. (2009, their Table 1), and the core designation of NGC 524, NGC 821, NGC 1374, NGC 3607, and NGC 5576 according to our Table 1. We also changed the designation of NGC 4552 from core-Sérsic to Sérsic following Bonfini et al. (2018), who claimed that the apparent core detected in this galaxy is because of the dust rings obstructing the light from the galactic center.

We used a constant 10% error on the velocity dispersion, and a 0.2 mag uncertainty on the absolute magnitude, i.e., a 20% error in the luminosity. Before performing the regression on the updated data-set, we checked to see if any single galaxies might bias the underlying relation defined by the bulk of the sample. This led us to exclude the Sérsic galaxy NGC 4482 from our regres-

¹² Kormendy & Bender (2013) pruned the data sample from Lauer et al. (2007) by excluding many dwarf ETGs which define the low-mass slope, and by excluding some lenticular galaxies while including other lenticular galaxies which had been misclassified as elliptical galaxies (see Graham 2019b).

¹³ These M32-type compact elliptical galaxies are M32, VCC 1192 (NGC 4467), VCC 1199, VCC 1297 (NGC 4486B), VCC 1440 (IC 798), VCC 1545 (IC 3509), and VCC 1627.

sions as it appears to have an underestimated velocity dispersion (Figure 12).

Figure 12 shows the V-band magnitude versus the velocity dispersion relation for Sérsic and core-Sérsic ETGs from the updated sample of Lauer et al. (2007). We obtain the bend-point at $\mathfrak{M}_V = -20.7$ mag (Vega), with 97 core-Sérsic ETGs defining the relation

$$\log(L_V) = (4.86 \pm 0.54) \log\left(\frac{\sigma}{200 \text{ km s}^{-1}}\right) + (8.52 \pm 0.07), \quad (11)$$

with $\Delta_{rms|L_V} = 0.37$ dex in the $\log L_V$ -direction, and 80 Sérsic ETGs defining a shallower relation given by,

$$\log(L_V) = (2.44 \pm 0.18) \log\left(\frac{\sigma}{200 \text{ km s}^{-1}}\right) + (8.41 \pm 0.04), \quad (12)$$

with $\Delta_{rms|L_V} = 0.31$ dex, obtained using the BCES(BISECTOR) regression¹⁴.

5.2. 3.6 μm Data-set

To probe the behavior of Sérsic and core-Sérsic ETGs in the L - σ diagram using near-infrared 3.6 μm -derived luminosities, we obtained the 3.6 μm absolute magnitudes for 73 ETGs from Sahu et al. (2019). This sample of 73 ETGs with 3.6 μm absolute magnitudes, has two galaxies (NGC 404, NGC 7457) common to our excluded sample (Section 3.1) and five galaxies (NGC 404, NGC 1316, NGC 2787, NGC 4342 and NGC 5128) common to the exclusions applied in Sahu et al. (2019, their Section 4). Hence, to maintain a consistency we exclude those galaxies in the $L_{3.6\mu\text{m}}-\sigma$ as well, which leaves us with a reduced 3.6 μm data-set of 67 ETGs. Checking for considerable outliers, we found that the core-Sérsic ETG NGC 4291 (shown in Figure 13 by a magenta-colored star), is a more than 2σ outlier, and significantly biases (changes the slope for) the best-fit line for core-Sérsic galaxies, hence we exclude NGC 4291 from the regression. The reduced 3.6 μm ETG sample is comprised of 42 Sérsic and 24 core-Sérsic ETGs.

Using our 3.6 μm data for ETGs, we recover the bend in the L - σ relation (Figure 13). Our core-Sérsic galaxies follow the relation

$$\log(L_{3.6\mu\text{m}}) = (5.16 \pm 0.53) \log\left(\frac{\sigma}{200 \text{ km s}^{-1}}\right) + (8.56 \pm 0.08), \quad (13)$$

with $\Delta_{rms|L_{3.6\mu\text{m}}} = 0.19$ dex (in the $\log L_{3.6\mu\text{m}}$ -direction) and Sérsic galaxies follow the shallower re-

lation,

$$\log(L_{3.6\mu\text{m}}) = (2.97 \pm 0.43) \log\left(\frac{\sigma}{200 \text{ km s}^{-1}}\right) + (8.72 \pm 0.07), \quad (14)$$

with $\Delta_{rms|L_{3.6\mu\text{m}}} = 0.36$ dex¹⁵.

The different exponent of the relations $L_B \propto \sigma^2$ (Graham & Soria 2019), $L_V \propto \sigma^{2.5}$ (Figure 12, Equation 12), and $L_{3.6\mu\text{m}} \propto \sigma^3$ (Figure 13, Equation 14) followed by Sérsic ETGs in different wavelength bands is consistent with the fact that they also follow a color-magnitude relation. Core-Sérsic ETGs, on the other hand, have roughly a constant color, suggesting similar slopes of the L - σ relation for all wavelength bands. The observed L - σ relations for core-Sérsic ETGs in different bands, i.e., $L_B \propto \sigma^{4-6}$ (Graham & Soria 2019), $L_V \propto \sigma^{4.9}$ (Figure 12, Equation 11), and $L_{3.6\mu\text{m}} \propto \sigma^{5.2}$ (Figure 13, Equation 13), are consistent as expected.

In the 3.6 μm magnitude ($\mathfrak{M}_{3.6\mu\text{m}}$) versus velocity dispersion diagram, we observe the bend-point at $\mathfrak{M}_{3.6\mu\text{m}} \approx -22.3$ mag in the AB magnitude system, which is $\mathfrak{M}_{3.6\mu\text{m}} \approx -25.1$ mag in the Vega magnitude system. Assuming a $B - 3.6\mu\text{m}$ color of ~ 5 (based on $B - K \approx 4$ and $K - 3.6\mu\text{m} \approx 1$), it seems to be consistent with the bend-point reported by previous studies at $\mathfrak{M}_B \approx -20.5$ mag (Graham & Soria 2019), $\mathfrak{M}_V \approx -21$ mag (Lauer et al. 2007), and $\mathfrak{M}_R \approx -22.17$ mag (Matković & Guzmán 2005).

In Sahu et al. (2019), we found that Sérsic and core-Sérsic ETGs follow the same $M_{BH} \propto M_{*,gal}^{1.65 \pm 0.11}$ relation. The relations $M_{BH} \propto \sigma^{4.95 \pm 0.38}$ for Sérsic ETGs (Equation 4) and $M_{BH} \propto \sigma^{8.64 \pm 1.10}$ for core-Sérsic galaxies (Equation 6), all of which are ETGs, combined with the above $M_{BH}-M_{*,gal}$ relation from Sahu et al. (2019) predict $M_{*,gal} \propto \sigma^{3.00 \pm 0.30}$ and $M_{*,gal} \propto \sigma^{5.24 \pm 0.75}$ for Sérsic and core-Sérsic ETGs, respectively. These two expected relations are consistent with what we have obtained (Equations 14 and 13, respectively) given that a constant stellar mass-to-light ratio of 0.6 ± 0.1 (Meidt et al. 2014) was used for 3.6 μm data in Sahu et al. (2019).

We have also plotted and performed regressions on our 26 LTGs (with 3.6 μm data from Davis et al. (2018)) in the $L_{3.6\mu\text{m}}-\sigma$ diagram, as shown in Figure 14. This sample of 26 LTGs, includes only one galaxy (NGC 5055) common to exclusions applied for our $M_{BH}-\sigma$ relations (described in Section 3.1). In addition to NGC 5055, we also exclude NGC 1300 as it is a considerable (more

¹⁴ Including NGC 4482 changes the Sérsic slope to 2.18 ± 0.25 , revealing that this single galaxy has a significant leverage on the slope of Sérsic population, hence it is better to exclude NGC 4482.

¹⁵ Including NGC 4291 in the regression changes the slope for the core-Sérsic galaxies to 5.94 ± 1.00 , proving that this one single outlier does affect the relation and hence it should remain excluded.

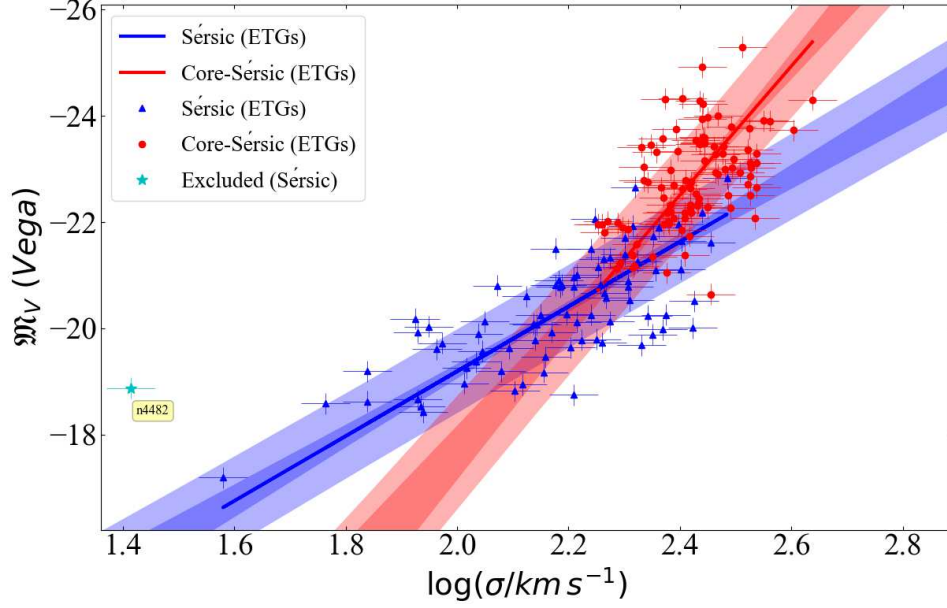


Figure 12. V-band absolute magnitude versus velocity dispersion diagram for Sérsic and core-Sérsic ETGs taken from the sample of Lauer et al. (2007). The BCES(BISECTOR) regression provides the relations $L_V \propto \sigma^{2.44 \pm 0.18}$ (Equation 12) and $L_V \propto \sigma^{4.86 \pm 0.54}$ (Equation 11) for Sérsic and core-Sérsic ETGs, respectively. This diagram suggests a broken $L-\sigma$ relation with the bend point at $M_V \approx -20.7$ mag (Vega).

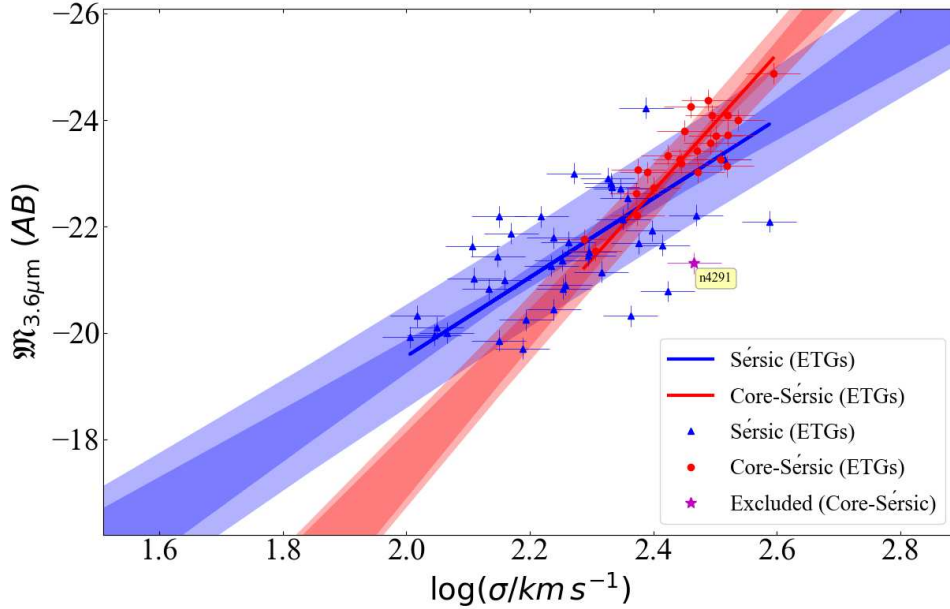


Figure 13. $3.6 \mu\text{m}$ absolute magnitude versus velocity dispersion for the Sérsic and core-Sérsic ETGs in our sample. We find the bend in the relation at $M_{3.6\mu\text{m}} \approx -22.3$ mag (AB) with Sérsic and core-Sérsic galaxies following the best-fit lines $L_{3.6\mu\text{m}} \propto \sigma^{3.01 \pm 0.42}$ (Equation 14) and $L_{3.6\mu\text{m}} \propto \sigma^{5.16 \pm 0.53}$ (Equation 13), respectively. The color-magnitude relation for Sérsic ETGs explains the different slope of $\sim 2.44 \pm 0.18$ in Figure 12 for the $L_V-\sigma$ relation.

than 2σ) outlier which can bias the relation for LTGs, as can be seen in Figure 14 with a cyan-colored star.

The reduced $3.6\ \mu\text{m}$ sample of 24 LTGs define the relation

$$\log(L_{3.6\mu\text{m}}) = (2.10 \pm 0.41) \log\left(\frac{\sigma}{200\ \text{km s}^{-1}}\right) + (8.90 \pm 0.09), \quad (15)$$

with $\Delta_{rms|L_{3.6\mu\text{m}}} = 0.20\ \text{dex}$ ¹⁶, consistent with the expected $M_{*,gal} \propto \sigma^{1.88 \pm 0.45}$ relation, derived from the relations $M_{BH} \propto M_{*,gal}^{3.05 \pm 0.70}$ (Davis et al. 2019) and $M_{BH} \propto \sigma^{5.75 \pm 0.34}$ (Equation 2). The slope of the L - σ relation that we derived for the LTGs, is also consistent with the B-band slope of 2.13 reported by Graham et al. (2019, see their Figure 7).

The parameters obtained from the asymmetric regression routines (BCES($Y|X$) and BCES($X|Y$)), for all the L - σ relations discussed above, are presented in Table 5 in the Appendix.

6. SOME MUSINGS ON SELECTION BIASES

The lack of directly measured low-mass SMBHs, due to the technological limitations to resolve their spheres-of-influence, poses a possible selection bias on the black hole mass scaling relations. In the past, several studies have discussed the consequences of, and possible solutions to, this sample selection bias (e.g., Batcheldor 2010; Graham et al. 2011; Shankar et al. 2016).

Batcheldor (2010) obtained an artificial M_{BH} - σ relation using simulated random M_{BH} and σ data, selected through the constraint of a best available resolution limit of $0''.1$ attainable from the *Hubble Space Telescope* (*HST*), for a maximum distance of 100 Mpc. The fake data produced the relation $\log(M_{BH}/M_{\odot}) = (4.0 \pm 0.3) \log(\sigma/200\ \text{km s}^{-1}) + (8.3 \pm 0.2)$, which was nearly consistent with the then observed M_{BH} - σ relation of Gültekin et al. (2009b). Batcheldor (2010) highlighted a crucial point for assessing the credibility of the observed black hole scaling relations. However, his relation with a slope of around 4 is lower than the steeper M_{BH} - σ relations based on larger samples of dynamically measured M_{BH} data (Graham et al. 2011; McConnell & Ma 2013; Graham & Scott 2013; Savorgnan & Graham 2015; Sabra et al. 2015).

Shankar et al. (2016) claim that galaxies which host a directly measured central SMBH have a higher velocity dispersion in comparison to other galaxies of similar stellar mass but without a direct SMBH measurement. Their claim is based on the offset they observed in the velocity dispersion versus galaxy stellar

mass diagram (σ - M_{STAR} , their Figure-1), between several samples of local ETGs with dynamically measured SMBH masses and a larger data-set of galaxies from Data Release-7 of the Sloan Digital Sky Survey (SDSS, York et al. 2000; Abazajian et al. 2009). This is restated in Shankar et al. (2019) with a slight change in their galaxy stellar masses based on the SDSS data they used.

Shankar et al. (2016) suggest that the offset they obtain is a consequence of a sample selection effect in which galaxies with low-mass BHs are excluded because it is not possible to resolve their spheres-of-influence due to technological limitations. They performed the comparison with the data from four different observational studies and provided a unified conclusion that galaxies hosting a directly-measured SMBH are offset in the σ - $M_{*,gal}$ relation, such that they have a higher σ relative to other similar mass galaxies. However, this is not completely true for all the data-sets they used and all of the galaxy stellar mass range in their plots. In their Figure-1, a significant number of data points from Savorgnan et al. (2016) overlap with the grey $\pm 1\sigma$ dispersion bands around the mean curve of the SDSS data, especially in the high-mass range $11 \lesssim \log(M_{*,gal}/M_{\odot}) \lesssim 12$. This can similarly be observed in Figure 1 of Shankar et al. (2019).

Interestingly, as described in Section 4, we have shown that Sérsic and core-Sérsic ETGs follow two distinct $M_{*,gal}$ - σ relations, consistent with Sérsic and core-Sérsic ETGs following two different M_{BH} - σ relations (Section 3.3), but a single M_{BH} - $M_{*,gal}$ relation (Sahu et al. 2019). Thus, we have two different relations in the σ - $M_{*,gal}$ diagram for Sérsic and core-Sérsic ETGs as shown in the left panel of Figure 15. The mean (black) curve from Shankar et al. (2016) lays within the $\pm 1\sigma$ scatter of the two relations followed by our Sérsic and core-Sérsic ETGs with directly-measured black hole masses, but outside of the more relevant darker (red and blue) bands denoting the $\pm 1\sigma$ uncertainty on the σ - $M_{*,gal}$ relations for ETGs with directly-measured black hole masses.

Upon inclusion of our LTGs (in the right panel of Figure 15), all of which are Sérsic galaxies, along with the (core-Sérsic and Sérsic) ETGs, we find that at the low-mass range, $10 \lesssim \log(M_{*,gal}/M_{\odot}) \lesssim 11$, their (black) curve resides between the two relations followed by our Sérsic ETGs (blue line) and LTGs (green line) which are primarily early-type (Sa-Sc) spiral galaxies. This suggests that their galaxy sample of ETGs may contain LTGs which could (partly) cause the offset.

In Shankar et al. (2016), the criteria for selecting only ETGs out of the exhaustive SDSS data-set was based

¹⁶ Including NGC 1300 in the regression changes the slope to 1.88 ± 0.48 .

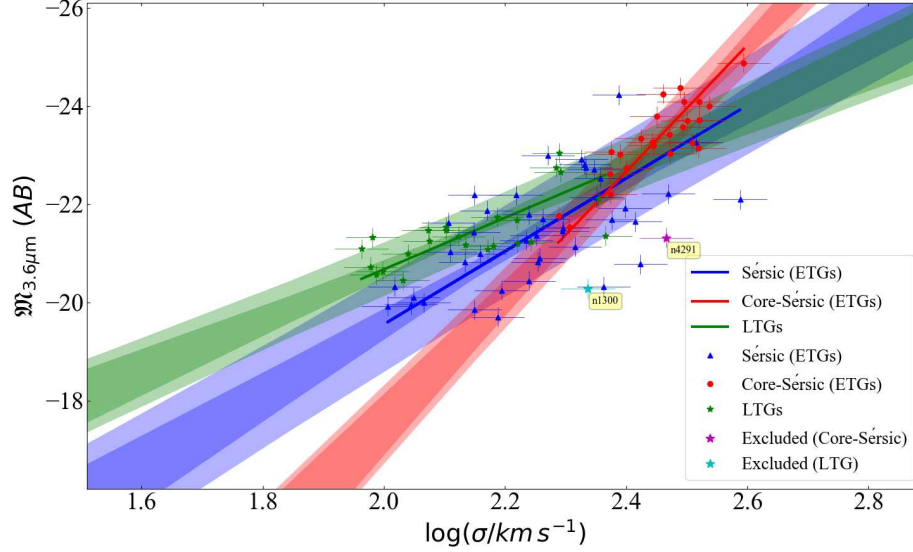


Figure 14. Similar to Figure 13 but including LTGs (spirals). All the spirals in our sample are Sérsic galaxies, and they also seem to define a tight correlation in the $L-\sigma$ diagram (Equation 15).

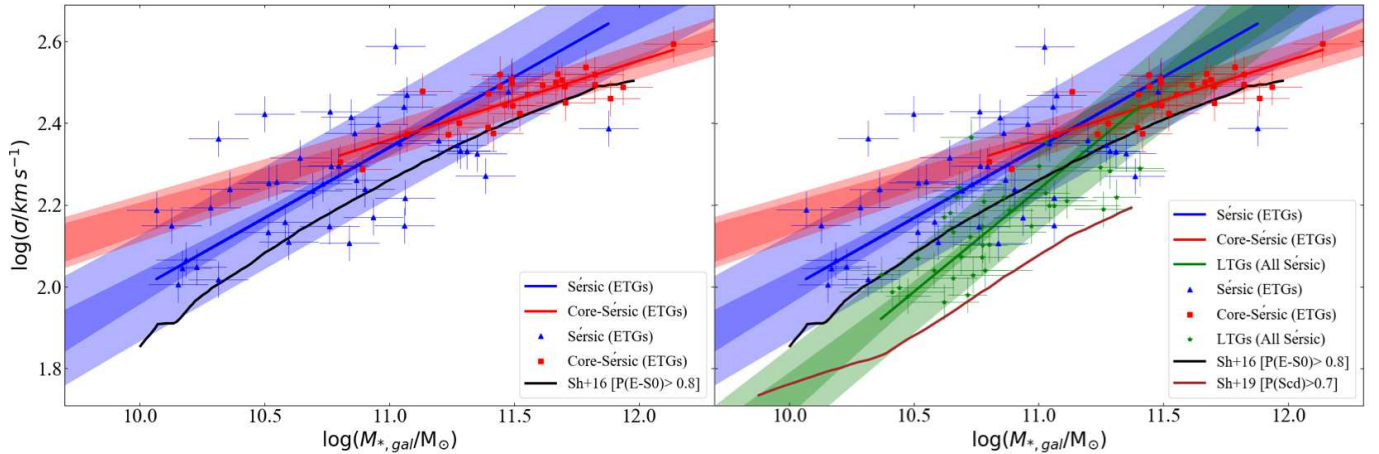


Figure 15. Velocity dispersion versus total galaxy stellar mass for Sérsic and core-Sérsic ETGs (left panel), and including LTGs, which are all Sérsic galaxies, in a separate panel for clarity. The mean $\sigma-M_{*,gal}$ distribution for (i) SDSS early-type galaxies from Shankar et al. (2016, their Figure 1) (black curve) and (ii) late spiral galaxies ($P(\text{Scd}) > 0.7$) from Shankar et al. (2019, their Figure 1) (brown curve) are shown. The brown curve resides below the relation defined by our LTG sample which are predominantly early (Sa-Sb) spirals. The black curve may reside below the relation defined by our ETG sample because of contamination by early spirals.

upon having a probability of greater than 0.8 for a galaxy being an E- or S0-type ($P(E - S0) \geq 0.8$). From the probabilities of galaxy types made available by Meert et al. (2015), we have calculated a $\sim 10\%$ contamination by spiral galaxies (LTGs) in the Shankar et al.’s ETG sample. Their best-fit $\sigma-M_{*,gal}$ relation’s position in-between the relation followed by our Sérsic ETGs and LTGs (right panel of Figure 15), coupled with their ETG

selection criteria based on probability, supports the suspicion that some of the offset may be due to spiral galaxy contamination in their SDSS ETG sample.

In the right-hand panel of Figure 15, we also include the brown curve for late spiral galaxies ($P(\text{Scd}) \geq 0.7$) from Shankar et al. (2019, see the left panel in their Figure 1), which lies below the relation defined by our predominantly early spiral galaxies (Sa-Sb), simply referred

to as LTGs in this paper. The various curves in Figure 15 represent the major morphological types. Their layering suggests that the apparent offset between galaxies with and without a directly measured black hole mass, as observed by Shankar et al. (2016, 2019), could simply be a reflection of the difference in the dominant morphological type in each sample. However, this is not conclusive and further investigation is required as their may yet be a selection bias or a discrepancy in the way that velocity dispersions are measured.

7. CONCLUSIONS AND IMPLICATIONS

Using the reduced sample of 137 galaxies with updated black hole masses and central stellar velocity dispersions, our work reveals sub-structure in the $M_{BH}-\sigma$ diagram due to galaxies with and without a core. Our previous galaxy decompositions (Savorgnan & Graham 2016; Davis et al. 2019; Sahu et al. 2019) have enabled us to accurately identify various structural components, such as intermediate or extended disks, bars, and partially-depleted stellar cores. This allowed us to search for substructures in the $M_{BH}-\sigma$ diagram, based on galaxy morphology, and also enabled us to clarify the situation regarding offset barred galaxies found in previous observational studies.

We performed and reported both symmetric BCES(BISECTOR) and asymmetric BCES($Y|X$) and BCES($X|Y$) regressions. The best-fit line obtained from the symmetric BCES(BISECTOR) regression is preferred because we are looking for a fundamental relation between two quantities (Feigelson & Babu 1992; Novak et al. 2006). For all our relations, we also obtained a symmetric (bisector) regression line using the MPFITEXY (modified FITEXY) routine, which are consistent with the corresponding BCES(BISECTOR) best-fit lines within the $\pm 1\sigma$ limits of the slopes and intercepts.

Our main results can be summarized as follows:

- The consistency between the best-fit lines for ETGs and LTGs in the M_{BH} versus σ diagram (Figure 1), suggests that ETGs and LTGs follow the same $M_{BH} \propto \sigma^{6.10 \pm 0.28}$ relation with a total scatter of $\Delta_{rms|BH} = 0.53$ dex, obtained using a single regression (Equation 3). However, this result depends on the galaxy sample and is somewhat misleading or limited. It is a fusion of substructures caused by (massive) core-Sérsic and (low-mass) Sérsic galaxies following two different $M_{BH}-\sigma$ relations.
- Core-Sérsic galaxies define the relation $M_{BH} \propto \sigma^{8.64 \pm 1.10}$ (Equation 6) and Sérsic galaxies define

the relation $M_{BH} \propto \sigma^{5.75 \pm 0.34}$ (Equation 5), with $\Delta_{rms|BH} = 0.46$ dex and $\Delta_{rms|BH} = 0.55$ dex, respectively. The inconsistency between the slopes of these two relations suggests two distinct relations in the $M_{BH}-\sigma$ diagram. The two lines intersect at $\sigma \approx 255 \text{ km s}^{-1}$ in Figure 4.

- We also detect a substructure in the $M_{BH}-\sigma$ diagram upon dividing our sample into galaxies with and without a stellar disk (Figures 5 and 6). However, this is likely because most of the elliptical ETGs are massive core-Sérsic galaxies, while most of the galaxies with a disk (ES, S0, and Sp-types) are Sérsic galaxies.
- We do not find any offset between the slope or intercept of the best-fit lines for barred and non-barred galaxies (Figures 7 and 8). We reveal that some previous studies noticed an offset in the intercepts between the $M_{BH}-\sigma$ relations for barred and non-barred galaxies partly because they relied on incomplete bar morphologies for several galaxies which failed to identify weak bars. Our previous image analysis improved upon this situation, and in our current larger sample we also have new galaxies with bars. Given that bars are known to elevate the velocity dispersion (Hartmann et al. 2014), this result begs further investigation, possibly folding in disc inclination, bar orientation to our line-of-sight, and rotational velocity.
- Galaxies with and without an AGN follow consistent relations in the $M_{BH}-\sigma$ diagram (Figure 11). Hence, the $M_{BH}-\sigma$ relations defined by Sérsic and core-Sérsic galaxies should be valid for a galaxy irrespective of whether or not its nucleus is active.
- Analyzing the $L-\sigma$ relation, based on V-band data from Lauer et al. (2007), our $3.6 \mu\text{m}$ data from Spitzer, and previously reported $L-\sigma$ relations using B- and R-bands, we investigated the $L-\sigma$ relation (Figures 12 and 13). We found that the relation between the luminosity of a galaxy and its central stellar velocity dispersion is bent due to core-Sérsic and Sérsic galaxies, analogous and consistent with the bend found in the $M_{BH}-\sigma$ relation and the $L-\mu_0$ relation (Graham & Guzmán 2003). Core-Sérsic galaxies follow the relation $L_V \propto \sigma^{4.86 \pm 0.54}$ and $L_{3.6 \mu\text{m}} \propto \sigma^{5.16 \pm 0.53}$ (Equations 11 and 13), whereas Sérsic galaxies follow the relation $L_V \propto \sigma^{2.44 \pm 0.18}$ and $L_{3.6 \mu\text{m}} \propto \sigma^{2.97 \pm 0.43}$ (Equations 12 and 14). The bend-point is consistent in the B-, V-, and $3.6 \mu\text{m}$ bands, corresponding to a stellar mass of $\approx 11 M_\odot$.

- The LTGs in our sample follow the relation $L_{3.6\mu\text{m}} \propto \sigma^{2.10 \pm 0.41}$ (Equation 15), and the $L_{3.6\mu\text{m}}-\sigma$ relations for Sérsic ETGs, core-Sérsic ETGs, and LTGs are internally consistent with our $M_{BH}-\sigma$ relations, and the $M_{BH}-M_{*,gal}$ relations from (Sahu et al. 2019).

Our $M_{BH}-\sigma$ (and $M_{BH}-M_{*,gal}$, and $M_{BH}-M_{*,sph}$) relations hold insights for theoretical studies into the co-evolution of black holes with their host galaxy properties (e.g., Volonteri & Ciotti 2013; Heckman & Best 2014), AGN feedback (Marconi et al. 2008), and the connection between black hole growth and star formation rates which have been found to depend on galaxy morphology (Calvi et al. 2018). Black hole mass scaling relations are also used to determine virial f -factors, for calculating AGN (black hole) masses (e.g., Onken et al. 2004; Graham et al. 2011; Bennert et al. 2011; Bentz & Katz 2015; Yu et al. 2019). Our $M_{BH}-\sigma$ relation due to Sérsic and core-Sérsic galaxies can be used to improve the virial f -factor based upon the galaxy core-type.

The new black hole mass scaling relations can be used to estimate the black hole masses of other galaxies using their easily measured properties, i.e., their galaxy stellar mass, spheroid/bulge stellar mass, or stellar velocity dispersion. These scaling relations, based on high resolution images of local ($z \sim 0$) galaxies, provide a benchmark for studies attempting to determine the evolution of the $M_{BH}-\sigma$ (or $M_{BH}-M_{*,gal}$ and $M_{BH}-M_{*,sph}$) relations (Woo et al. 2006; Salviander et al. 2007; Bennert et al. 2011; Hiner 2012; Sexton et al. 2019). Moreover, given the different scaling relations based on the galaxy sub-morphologies, care should be taken in regard to the galaxy types present in one's sample. For distant galaxies where it is difficult to perform multi-component decompositions to obtain bulge masses and extract detailed morphologies, $M_{BH}-M_{*,gal}$ relations can be used provided ETG or LTG classifications are known because ETGs and LTGs follow two different $M_{BH}-M_{*,gal}$ relations (Sahu et al. 2019).

Similarly, as it might be difficult to detect the (depleted) core in distant galaxies, the single regression $M_{BH}-\sigma$ relation presented in this paper (Equation 3) can be used. However, if one is primarily sampling massive distant galaxies, with $\sigma \gtrsim 255\text{kms}^{-1}$, it would be preferable to compare that data with the core-Sérsic $M_{BH}-\sigma$ relation, or risk inferring a false evolution if using the shallower relation.

Our scaling relations can be used to estimate black hole masses for a large data-set of galaxies to obtain the black hole mass function in the local Universe (McLure & Dunlop 2004; Shankar et al. 2004; Graham et al. 2007). This can be used to improve the predictions of the amplitude and frequency of ground-based detections of long-wavelength gravitational waves, produced by merging SMBHs, using pulsar timing arrays (Shannon et al. 2015; Hobbs & Dai 2017) and also MeerKAT (Jonas 2007). Furthermore, these scaling relations can also be used to constrain the space-based detection of long-wavelength gravitational waves by the Laser Interferometer Space Antenna (LISA, Danzmann 2017), and beyond LISA (bLISA, Baker et al. 2019).

ACKNOWLEDGMENTS

We thank the anonymous referee whose comments helped to increase the clarity of this paper. This research was conducted with the Australian Research Council Centre of Excellence for Gravitational Wave Discovery (OzGrav), through project number CE170100004. AWG was supported under the Australian Research Council's funding scheme DP17012923. This work has made use of the NASA/IPAC Infrared Science Archive and the NASA/IPAC Extragalactic Database (NED). This research has also made use of the Two Micron All Sky Survey and Sloan Digital Sky Survey database. We also acknowledge the use of the HYPERLEDA database <http://leda.univ-lyon1.fr>.

REFERENCES

- Abazajian, K. N., Adelman-McCarthy, J. K., Agüeros, M. A., et al. 2009, ApJS, 182, 543, doi: [10.1088/0067-0049/182/2/543](https://doi.org/10.1088/0067-0049/182/2/543)
- Akritas, M. G., & Bershadsky, M. A. 1996, ApJ, 470, 706, doi: [10.1086/177901](https://doi.org/10.1086/177901)
- Baker, J., Barke, S. F., Bender, P. L., et al. 2019, arXiv e-prints, arXiv:1907.11305. <https://arxiv.org/abs/1907.11305>
- Batcheldor, D. 2010, ApJL, 711, L108, doi: [10.1088/2041-8205/711/2/L108](https://doi.org/10.1088/2041-8205/711/2/L108)
- Batcheldor, D., Robinson, A., Axon, D. J., Perlman, E. S., & Merritt, D. 2010, ApJ, 717, L6, doi: [10.1088/2041-8205/717/1/L6](https://doi.org/10.1088/2041-8205/717/1/L6)
- Bedregal, A. G., Aragón-Salamanca, A., & Merrifield, M. R. 2006, MNRAS, 373, 1125, doi: [10.1111/j.1365-2966.2006.11031.x](https://doi.org/10.1111/j.1365-2966.2006.11031.x)

- Begelman, M. C., Blandford, R. D., & Rees, M. J. 1980, *Nature*, 287, 307, doi: [10.1038/287307a0](https://doi.org/10.1038/287307a0)
- Bellstedt, S., Graham, A. W., Forbes, D. A., et al. 2017, *MNRAS*, 470, 1321, doi: [10.1093/mnras/stx1348](https://doi.org/10.1093/mnras/stx1348)
- Bennert, V. N., Auger, M. W., Treu, T., Woo, J.-H., & Malkan, M. A. 2011, *ApJ*, 726, 59, doi: [10.1088/0004-637X/726/2/59](https://doi.org/10.1088/0004-637X/726/2/59)
- Bennert, V. N., Treu, T., Auger, M. W., et al. 2015, *ApJ*, 809, 20, doi: [10.1088/0004-637X/809/1/20](https://doi.org/10.1088/0004-637X/809/1/20)
- Bentz, M. C., & Katz, S. 2015, *PASP*, 127, 67, doi: [10.1086/679601](https://doi.org/10.1086/679601)
- Binney, J. 1982, *ARA&A*, 20, 399, doi: [10.1146/annurev.aa.20.090182.002151](https://doi.org/10.1146/annurev.aa.20.090182.002151)
- Blom, C., Forbes, D. A., Foster, C., Romanowsky, A. J., & Brodie, J. P. 2014, *MNRAS*, 439, 2420, doi: [10.1093/mnras/stu095](https://doi.org/10.1093/mnras/stu095)
- Bogdán, Á., Lovisari, L., Volonteri, M., & Dubois, Y. 2018, *ApJ*, 852, 131, doi: [10.3847/1538-4357/aa9ab5](https://doi.org/10.3847/1538-4357/aa9ab5)
- Boizelle, B. D., Barth, A. J., Walsh, J. L., et al. 2019, arXiv e-prints, arXiv:1906.06267. <https://arxiv.org/abs/1906.06267>
- Bonfini, P., González-Martín, O., Fritz, J., et al. 2018, *MNRAS*, 478, 1161, doi: [10.1093/mnras/sty1087](https://doi.org/10.1093/mnras/sty1087)
- Brown, J. S., Valluri, M., Shen, J., & Debattista, V. P. 2013, *ApJ*, 778, 151, doi: [10.1088/0004-637X/778/2/151](https://doi.org/10.1088/0004-637X/778/2/151)
- Buta, R. J., Sheth, K., Regan, M., et al. 2010, *ApJS*, 190, 147, doi: [10.1088/0067-0049/190/1/147](https://doi.org/10.1088/0067-0049/190/1/147)
- Calvi, R., Vulcani, B., Poggianti, B. M., et al. 2018, *MNRAS*, 481, 3456, doi: [10.1093/mnras/sty2476](https://doi.org/10.1093/mnras/sty2476)
- Cappellari, M., Bacon, R., Bureau, M., et al. 2006, *MNRAS*, 366, 1126, doi: [10.1111/j.1365-2966.2005.09981.x](https://doi.org/10.1111/j.1365-2966.2005.09981.x)
- Ciambur, B. C. 2015, *ApJ*, 810, 120, doi: [10.1088/0004-637X/810/2/120](https://doi.org/10.1088/0004-637X/810/2/120)
- . 2016, *PASA*, 33, e062, doi: [10.1017/pasa.2016.60](https://doi.org/10.1017/pasa.2016.60)
- Ciotti, L., & van Albada, T. S. 2001, *ApJL*, 552, L13, doi: [10.1086/320260](https://doi.org/10.1086/320260)
- Combes, F., García-Burillo, S., Audibert, A., et al. 2019, *A&A*, 623, A79, doi: [10.1051/0004-6361/201834560](https://doi.org/10.1051/0004-6361/201834560)
- Dalla Bontà, E., Ferrarese, L., Corsini, E. M., et al. 2009, *ApJ*, 690, 537, doi: [10.1088/0004-637X/690/1/537](https://doi.org/10.1088/0004-637X/690/1/537)
- Danzmann, K. 2017, in *Society of Photo-Optical Instrumentation Engineers (SPIE) Conference Series*, Vol. 10566, Proc. SPIE, 1056610, doi: [10.1117/12.2308272](https://doi.org/10.1117/12.2308272)
- Davies, R. L., et al. 1983, *ApJ*, 266, 41, doi: [10.1086/160757](https://doi.org/10.1086/160757)
- Davis, B. L., Graham, A. W., & Cameron, E. 2018, *ApJ*, 869, 113, doi: [10.3847/1538-4357/aae820](https://doi.org/10.3847/1538-4357/aae820)
- Davis, B. L., Graham, A. W., & Cameron, E. 2019, *ApJ*, 873, 85, doi: [10.3847/1538-4357/aaf3b8](https://doi.org/10.3847/1538-4357/aaf3b8)
- Davis, B. L., Graham, A. W., & Seigar, M. S. 2017, *MNRAS*, 471, 2187, doi: [10.1093/mnras/stx1794](https://doi.org/10.1093/mnras/stx1794)
- de Rijcke, S., Michielsen, D., Dejonghe, H., Zeilinger, W. W., & Hau, G. K. T. 2005, *A&A*, 438, 491, doi: [10.1051/0004-6361:20042213](https://doi.org/10.1051/0004-6361:20042213)
- de Vaucouleurs, G., de Vaucouleurs, A., Corwin, Herold G., J., et al. 1991, *Third Reference Catalogue of Bright Galaxies*
- Dullo, B. T. 2014, in *Astronomical Society of the Pacific Conference Series*, Vol. 480, *Structure and Dynamics of Disk Galaxies*, ed. M. S. Seigar & P. Treuthardt, 75
- Dullo, B. T., & Graham, A. W. 2013, *ApJ*, 768, 36, doi: [10.1088/0004-637X/768/1/36](https://doi.org/10.1088/0004-637X/768/1/36)
- . 2014, *MNRAS*, 444, 2700, doi: [10.1093/mnras/stu1590](https://doi.org/10.1093/mnras/stu1590)
- Erwin, P., Saglia, R. P., Fabricius, M., et al. 2015, *MNRAS*, 446, 4039, doi: [10.1093/mnras/stu2376](https://doi.org/10.1093/mnras/stu2376)
- Eskridge, P. B., Frogel, J. A., Pogge, R. W., et al. 2000, *AJ*, 119, 536, doi: [10.1086/301203](https://doi.org/10.1086/301203)
- Event Horizon Telescope Collaboration, Akiyama, K., Alberdi, A., et al. 2019, *ApJ*, 875, L6, doi: [10.3847/2041-8213/ab1141](https://doi.org/10.3847/2041-8213/ab1141)
- Faber, S. M., & Jackson, R. E. 1976, *ApJ*, 204, 668, doi: [10.1086/154215](https://doi.org/10.1086/154215)
- Fabian, A. C. 1999, *MNRAS*, 308, L39, doi: [10.1046/j.1365-8711.1999.03017.x](https://doi.org/10.1046/j.1365-8711.1999.03017.x)
- Farouki, R. T., Shapiro, S. L., & Duncan, M. J. 1983, *ApJ*, 265, 597, doi: [10.1086/160704](https://doi.org/10.1086/160704)
- Feigelson, E. D., & Babu, G. J. 1992, *ApJ*, 397, 55, doi: [10.1086/171766](https://doi.org/10.1086/171766)
- Ferrarese, L., & Ford, H. 2005, *SSRv*, 116, 523, doi: [10.1007/s11214-005-3947-6](https://doi.org/10.1007/s11214-005-3947-6)
- Ferrarese, L., & Merritt, D. 2000, *ApJ*, 539, L9, doi: [10.1086/312838](https://doi.org/10.1086/312838)
- Gebhardt, K., Bender, R., Bower, G., et al. 2000, *ApJ*, 539, L13, doi: [10.1086/312840](https://doi.org/10.1086/312840)
- Graham, A. 2007, in *Bulletin of the American Astronomical Society*, Vol. 39, *American Astronomical Society Meeting Abstracts*, 759
- Graham, A. W. 2008a, *PASA*, 25, 167, doi: [10.1071/AS08013](https://doi.org/10.1071/AS08013)
- . 2008b, *ApJ*, 680, 143, doi: [10.1086/587473](https://doi.org/10.1086/587473)
- Graham, A. W. 2014, in *Astronomical Society of the Pacific Conference Series*, Vol. 480, *Structure and Dynamics of Disk Galaxies*, ed. M. S. Seigar & P. Treuthardt, 185. <https://arxiv.org/abs/1311.7207>
- Graham, A. W. 2016, in *Astrophysics and Space Science Library*, Vol. 418, *Galactic Bulges*, ed. E. Laurikainen, R. Peletier, & D. Gadotti, 263, doi: [10.1007/978-3-319-19378-6_11](https://doi.org/10.1007/978-3-319-19378-6_11)
- . 2019a, *MNRAS*, 1547, doi: [10.1093/mnras/stz1623](https://doi.org/10.1093/mnras/stz1623)

- . 2019b, PASA, 36, e035, doi: [10.1017/pasa.2019.23](https://doi.org/10.1017/pasa.2019.23)
- Graham, A. W., Ciambur, B. C., & Savorgnan, G. A. D. 2016a, ApJ, 831, 132, doi: [10.3847/0004-637X/831/2/132](https://doi.org/10.3847/0004-637X/831/2/132)
- Graham, A. W., & Driver, S. P. 2007, ApJ, 655, 77, doi: [10.1086/509758](https://doi.org/10.1086/509758)
- Graham, A. W., Durré, M., Savorgnan, G. A. D., et al. 2016b, ApJ, 819, 43, doi: [10.3847/0004-637X/819/1/43](https://doi.org/10.3847/0004-637X/819/1/43)
- Graham, A. W., & Guzmán, R. 2003, AJ, 125, 2936, doi: [10.1086/374992](https://doi.org/10.1086/374992)
- Graham, A. W., & Scott, N. 2013, ApJ, 764, 151, doi: [10.1088/0004-637X/764/2/151](https://doi.org/10.1088/0004-637X/764/2/151)
- Graham, A. W., & Soria, R. 2019, MNRAS, 484, 794, doi: [10.1093/mnras/sty3398](https://doi.org/10.1093/mnras/sty3398)
- Graham, A. W., Soria, R., & Davis, B. L. 2019, MNRAS, 484, 814, doi: [10.1093/mnras/sty3068](https://doi.org/10.1093/mnras/sty3068)
- Graham, A. W., et al. 2003, AJ, 125, 2951, doi: [10.1086/375320](https://doi.org/10.1086/375320)
- . 2007, MNRAS, 378, 198, doi: [10.1111/j.1365-2966.2007.11770.x](https://doi.org/10.1111/j.1365-2966.2007.11770.x)
- . 2011, MNRAS, 412, 2211, doi: [10.1111/j.1365-2966.2010.18045.x](https://doi.org/10.1111/j.1365-2966.2010.18045.x)
- Greene, J. E., & Ho, L. C. 2006, ApJL, 641, L21, doi: [10.1086/500507](https://doi.org/10.1086/500507)
- Greene, J. E., Peng, C. Y., Kim, M., et al. 2010, ApJ, 721, 26, doi: [10.1088/0004-637X/721/1/26](https://doi.org/10.1088/0004-637X/721/1/26)
- Greene, J. E., Seth, A., Kim, M., et al. 2016, ApJ, 826, L32, doi: [10.3847/2041-8205/826/2/L32](https://doi.org/10.3847/2041-8205/826/2/L32)
- Gültekin, K., Gebhardt, K., Kormendy, J., et al. 2014, ApJ, 781, 112, doi: [10.1088/0004-637X/781/2/112](https://doi.org/10.1088/0004-637X/781/2/112)
- Gültekin, K., Richstone, D. O., Gebhardt, K., et al. 2009a, ApJ, 698, 198, doi: [10.1088/0004-637X/698/1/198](https://doi.org/10.1088/0004-637X/698/1/198)
- . 2009b, ApJ, 695, 1577, doi: [10.1088/0004-637X/695/2/1577](https://doi.org/10.1088/0004-637X/695/2/1577)
- Hartmann, M., Debattista, V. P., Cole, D. R., et al. 2014, MNRAS, 441, 1243, doi: [10.1093/mnras/stu627](https://doi.org/10.1093/mnras/stu627)
- Heckman, T. M., & Best, P. N. 2014, ARA&A, 52, 589, doi: [10.1146/annurev-astro-081913-035722](https://doi.org/10.1146/annurev-astro-081913-035722)
- Held, E. V., de Zeeuw, T., Mould, J., & Picard, A. 1992, AJ, 103, 851, doi: [10.1086/116106](https://doi.org/10.1086/116106)
- Hilz, M., Naab, T., & Ostriker, J. P. 2013, MNRAS, 429, 2924, doi: [10.1093/mnras/sts501](https://doi.org/10.1093/mnras/sts501)
- Hiner, K. D. 2012, PhD thesis, University of California, Riverside
- Hobbs, G., & Dai, S. 2017, arXiv e-prints, arXiv:1707.01615. <https://arxiv.org/abs/1707.01615>
- Hu, J. 2008, MNRAS, 386, 2242, doi: [10.1111/j.1365-2966.2008.13195.x](https://doi.org/10.1111/j.1365-2966.2008.13195.x)
- Huré, J. M., Hersant, F., Surville, C., Nakai, N., & Jacq, T. 2011, A&A, 530, A145, doi: [10.1051/0004-6361/201015062](https://doi.org/10.1051/0004-6361/201015062)
- Jonas, J. 2007, in From Planets to Dark Energy: the Modern Radio Universe, 7
- Jorgensen, I., Franx, M., & Kjaergaard, P. 1995, MNRAS, 276, 1341, doi: [10.1093/mnras/276.4.1341](https://doi.org/10.1093/mnras/276.4.1341)
- King, I. R., & Minkowski, R. 1966, ApJ, 143, 1002, doi: [10.1086/148580](https://doi.org/10.1086/148580)
- King, I. R., & Minkowski, R. 1972, in IAU Symposium, Vol. 44, External Galaxies and Quasi-Stellar Objects, ed. D. S. Evans, D. Wills, & B. J. Wills, 87
- Kormendy, J., & Bender, R. 2013, ApJ, 769, L5, doi: [10.1088/2041-8205/769/1/L5](https://doi.org/10.1088/2041-8205/769/1/L5)
- Kormendy, J., Fisher, D. B., Cornell, M. E., & Bender, R. 2009, ApJS, 182, 216, doi: [10.1088/0067-0049/182/1/216](https://doi.org/10.1088/0067-0049/182/1/216)
- Kormendy, J., & Ho, L. C. 2013, Annual Review of Astronomy and Astrophysics, 51, 511, doi: [10.1146/annurev-astro-082708-101811](https://doi.org/10.1146/annurev-astro-082708-101811)
- Kormendy, J., & Kennicutt, Robert C., J. 2004, ARA&A, 42, 603, doi: [10.1146/annurev.astro.42.053102.134024](https://doi.org/10.1146/annurev.astro.42.053102.134024)
- Lauer, T. R., Faber, S. M., Richstone, D., et al. 2007, ApJ, 662, 808, doi: [10.1086/518223](https://doi.org/10.1086/518223)
- Liller, M. H. 1966, ApJ, 146, 28, doi: [10.1086/148857](https://doi.org/10.1086/148857)
- Malumuth, E. M., & Kirshner, R. P. 1981, ApJ, 251, 508, doi: [10.1086/159490](https://doi.org/10.1086/159490)
- Marconi, A., Axon, D. J., Maiolino, R., et al. 2008, ApJ, 678, 693, doi: [10.1086/529360](https://doi.org/10.1086/529360)
- Markwardt, C. 2012, MPFIT: Robust non-linear least squares curve fitting. <http://ascl.net/1208.019>
- Matković, A., & Guzmán, R. 2005, MNRAS, 362, 289, doi: [10.1111/j.1365-2966.2005.09298.x](https://doi.org/10.1111/j.1365-2966.2005.09298.x)
- McConnell, N. J., & Ma, C.-P. 2013, ApJ, 764, 184, doi: [10.1088/0004-637X/764/2/184](https://doi.org/10.1088/0004-637X/764/2/184)
- McLure, R. J., & Dunlop, J. S. 2004, MNRAS, 352, 1390, doi: [10.1111/j.1365-2966.2004.08034.x](https://doi.org/10.1111/j.1365-2966.2004.08034.x)
- Meert, A., Vikram, V., & Bernardi, M. 2015, MNRAS, 446, 3943, doi: [10.1093/mnras/stu2333](https://doi.org/10.1093/mnras/stu2333)
- Mehrgan, K., Thomas, J., Saglia, R., et al. 2019, arXiv e-prints, arXiv:1907.10608. <https://arxiv.org/abs/1907.10608>
- Meidt, S. E., Schinnerer, E., van de Ven, G., et al. 2014, ApJ, 788, 144, doi: [10.1088/0004-637X/788/2/144](https://doi.org/10.1088/0004-637X/788/2/144)
- Merritt, D., & Ferrarese, L. 2001, ApJ, 547, 140, doi: [10.1086/318372](https://doi.org/10.1086/318372)
- Merritt, D., & Milosavljević, M. 2005, Living Reviews in Relativity, 8, 8, doi: [10.12942/lrr-2005-8](https://doi.org/10.12942/lrr-2005-8)
- Minkowski, R. 1962, in IAU Symposium, Vol. 15, Problems of Extra-Galactic Research, ed. G. C. McVittie, 112
- Molaeinezhad, A., Zhu, L., Falcón-Barroso, J., et al. 2019, MNRAS, 488, 1012, doi: [10.1093/mnras/stz1776](https://doi.org/10.1093/mnras/stz1776)
- Nemmen, R. S., Georganopoulos, M., Guiriec, S., et al. 2012, Science, 338, 1445, doi: [10.1126/science.1227416](https://doi.org/10.1126/science.1227416)

- Nguyen, D. D., Seth, A. C., den Brok, M., et al. 2017, *ApJ*, 836, 237, doi: [10.3847/1538-4357/aa5cb4](https://doi.org/10.3847/1538-4357/aa5cb4)
- Nguyen, D. D., Seth, A. C., Neumayer, N., et al. 2018, *ApJ*, 858, 118, doi: [10.3847/1538-4357/aabe28](https://doi.org/10.3847/1538-4357/aabe28)
- Nguyen, D. D., den Brok, M., Seth, A. C., et al. 2019, arXiv e-prints, arXiv:1902.03813, <https://arxiv.org/abs/1902.03813>
- Novak, G. S., Faber, S. M., & Dekel, A. 2006, *ApJ*, 637, 96, doi: [10.1086/498333](https://doi.org/10.1086/498333)
- Nowak, N., Saglia, R. P., Thomas, J., et al. 2007, *MNRAS*, 379, 909, doi: [10.1111/j.1365-2966.2007.11949.x](https://doi.org/10.1111/j.1365-2966.2007.11949.x)
- Onken, C. A., Ferrarese, L., Merritt, D., et al. 2004, *ApJ*, 615, 645, doi: [10.1086/424655](https://doi.org/10.1086/424655)
- Oser, L., Naab, T., Ostriker, J. P., & Johansson, P. H. 2012, *ApJ*, 744, 63, doi: [10.1088/0004-637X/744/1/63](https://doi.org/10.1088/0004-637X/744/1/63)
- Paturel, G., Petit, C., Prugniel, P., et al. 2003, *A&A*, 412, 45, doi: [10.1051/0004-6361:20031411](https://doi.org/10.1051/0004-6361:20031411)
- Press, W. H., Teukolsky, S. A., Vetterling, W. T., & Flannery, B. P. 1992, *Numerical recipes in FORTRAN. The art of scientific computing*
- Sabra, B. M., Saliba, C., Abi Akl, M., & Chahine, G. 2015, *ApJ*, 803, 5, doi: [10.1088/0004-637X/803/1/5](https://doi.org/10.1088/0004-637X/803/1/5)
- Saglia, R. P., Opitsch, M., Erwin, P., et al. 2016, *ApJ*, 818, 47, doi: [10.3847/0004-637X/818/1/47](https://doi.org/10.3847/0004-637X/818/1/47)
- Sahu, N., Graham, A. W., & Davis, B. L. 2019, *ApJ*, 876, 155, doi: [10.3847/1538-4357/ab0f32](https://doi.org/10.3847/1538-4357/ab0f32)
- Salviander, S., Shields, G. A., Gebhardt, K., & Bonning, E. W. 2007, *ApJ*, 662, 131, doi: [10.1086/513086](https://doi.org/10.1086/513086)
- Savognan, G. A. D., & Graham, A. W. 2015, *MNRAS*, 446, 2330, doi: [10.1093/mnras/stu2259](https://doi.org/10.1093/mnras/stu2259)
- Savognan, G. A. D., & Graham, A. W. 2016, *ApJS*, 222, 10, doi: [10.3847/0067-0049/222/1/10](https://doi.org/10.3847/0067-0049/222/1/10)
- Savognan, G. A. D., et al. 2016, *ApJ*, 817, 21, doi: [10.3847/0004-637X/817/1/21](https://doi.org/10.3847/0004-637X/817/1/21)
- Schechter, P. L. 1980, *AJ*, 85, 801, doi: [10.1086/112742](https://doi.org/10.1086/112742)
- Sérsic, J. L. 1963, *BAAA*, 6, 41
- Sexton, R. O., Canalizo, G., Hiner, K. D., et al. 2019, *ApJ*, 878, 101, doi: [10.3847/1538-4357/ab21d5](https://doi.org/10.3847/1538-4357/ab21d5)
- Shankar, F., Marulli, F., Bernardi, M., et al. 2013, *MNRAS*, 428, 109, doi: [10.1093/mnras/sts001](https://doi.org/10.1093/mnras/sts001)
- Shankar, F., Salucci, P., Granato, G. L., De Zotti, G., & Danese, L. 2004, *MNRAS*, 354, 1020, doi: [10.1111/j.1365-2966.2004.08261.x](https://doi.org/10.1111/j.1365-2966.2004.08261.x)
- Shankar, F., Bernardi, M., Sheth, R. K., et al. 2016, *MNRAS*, 460, 3119, doi: [10.1093/mnras/stw678](https://doi.org/10.1093/mnras/stw678)
- Shankar, F., Bernardi, M., Richardson, K., et al. 2019, *MNRAS*, 485, 1278, doi: [10.1093/mnras/stz376](https://doi.org/10.1093/mnras/stz376)
- Shannon, R. M., Ravi, V., Lentati, L. T., et al. 2015, *Science*, 349, 1522, doi: [10.1126/science.aab1910](https://doi.org/10.1126/science.aab1910)
- Silk, J., & Rees, M. J. 1998, *A&A*, 331, L1, <https://arxiv.org/abs/astro-ph/9801013>
- Thater, S., Krajinovic, D., Cappellari, M., et al. 2019, arXiv e-prints, <https://arxiv.org/abs/1902.10175>
- Thomas, J., Ma, C.-P., McConnell, N. J., et al. 2016, *Nature*, 532, 340, doi: [10.1038/nature17197](https://doi.org/10.1038/nature17197)
- Tonry, J. L. 1981, *ApJL*, 251, L1, doi: [10.1086/183681](https://doi.org/10.1086/183681)
- Tremaine, S., Gebhardt, K., Bender, R., et al. 2002, *ApJ*, 574, 740, doi: [10.1086/341002](https://doi.org/10.1086/341002)
- van den Bosch, R. C. E. 2016, *ApJ*, 831, 134, doi: [10.3847/0004-637X/831/2/134](https://doi.org/10.3847/0004-637X/831/2/134)
- Véron-Cetty, M. P., & Véron, P. 2010, *A&A*, 518, A10, doi: [10.1051/0004-6361/201014188](https://doi.org/10.1051/0004-6361/201014188)
- Volonteri, M., & Ciotti, L. 2013, *ApJ*, 768, 29, doi: [10.1088/0004-637X/768/1/29](https://doi.org/10.1088/0004-637X/768/1/29)
- Walsh, J. L., van den Bosch, R. C. E., Gebhardt, K., et al. 2015, *ApJ*, 808, 183, doi: [10.1088/0004-637X/808/2/183](https://doi.org/10.1088/0004-637X/808/2/183)
- Williams, M. J., Bureau, M., & Cappellari, M. 2010, *MNRAS*, 409, 1330, doi: [10.1111/j.1365-2966.2010.17406.x](https://doi.org/10.1111/j.1365-2966.2010.17406.x)
- Woo, J.-H., Schulze, A., Park, D., et al. 2013, *ApJ*, 772, 49, doi: [10.1088/0004-637X/772/1/49](https://doi.org/10.1088/0004-637X/772/1/49)
- Woo, J.-H., Treu, T., Malkan, M. A., & Blandford, R. D. 2006, *ApJ*, 645, 900, doi: [10.1086/504586](https://doi.org/10.1086/504586)
- York, D. G., Adelman, J., Anderson, John E., J., et al. 2000, *AJ*, 120, 1579, doi: [10.1086/301513](https://doi.org/10.1086/301513)
- Yu, L.-M., Bian, W.-H., Wang, C., Zhao, B.-X., & Ge, X. 2019, *MNRAS*, 488, 1519, doi: [10.1093/mnras/stz1766](https://doi.org/10.1093/mnras/stz1766)

APPENDIX

Table 3. Black Hole Mass versus Velocity Dispersion [$\log(M_{BH}/M_{\odot}) = \alpha \log(\sigma/200) + \beta$]

Regression	Minimization	α	β	ϵ	$\Delta_{rms BH}$	r	r_s
(1)	(2)	(3)	(dex) (4)	(dex) (5)	(dex) (6)	(7)	(8)
Early-Type and Late-Type Galaxies							
91 Early-Type Galaxies							
BCES(<i>Bisector</i>)	<i>Symmetric</i>	5.71 ± 0.33	8.32 ± 0.05	0.32	0.44	} 0.86	0.85
BCES($M_{BH} \sigma$)	M_{BH}	5.22 ± 0.36	8.34 ± 0.05	0.32	0.43		
BCES(σM_{BH})	σ	6.29 ± 0.35	8.29 ± 0.06	0.34	0.47		
46 Late-Type Galaxies							
BCES(<i>Bisector</i>)	<i>Symmetric</i>	5.82 ± 0.75	8.17 ± 0.14	0.57	0.63	} 0.59	0.49
BCES($M_{BH} \sigma$)	M_{BH}	4.07 ± 0.90	7.90 ± 0.17	0.54	0.58		
BCES(σM_{BH})	σ	10.06 ± 1.74	8.83 ± 0.30	0.85	0.96		
Single Regression on (137) Early and Late-Type Galaxies							
BCES(<i>Bisector</i>)	<i>Symmetric</i>	6.10 ± 0.28	8.27 ± 0.04	0.43	0.53	} 0.86	0.87
BCES($M_{BH} \sigma$)	M_{BH}	5.50 ± 0.29	8.26 ± 0.04	0.42	0.51		
BCES(σM_{BH})	σ	6.82 ± 0.32	8.29 ± 0.05	0.46	0.58		
Sérsic and Core-Sérsic Galaxies							
102 Sérsic Galaxies							
BCES(<i>Bisector</i>)	<i>Symmetric</i>	5.75 ± 0.34	8.24 ± 0.05	0.46	0.55	} 0.78	0.78
BCES($M_{BH} \sigma$)	M_{BH}	4.86 ± 0.34	8.16 ± 0.05	0.45	0.52		
BCES(σM_{BH})	σ	7.02 ± 0.52	8.34 ± 0.07	0.54	0.64		
35 Core-Sérsic Galaxies							
BCES(<i>Bisector</i>)	<i>Symmetric</i>	8.64 ± 1.10	7.91 ± 0.20	0.25	0.46	} 0.73	0.65
BCES($M_{BH} \sigma$)	M_{BH}	7.74 ± 1.15	8.04 ± 0.18	0.25	0.43		
BCES(σM_{BH})	σ	9.77 ± 1.70	7.74 ± 0.31	0.27	0.52		
Galaxies with and without a disk							
93 ES, S0, Sp-Type Galaxies							
BCES(<i>Bisector</i>)	<i>Symmetric</i>	5.72 ± 0.34	8.22 ± 0.06	0.47	0.56	} 0.79	0.78
BCES($M_{BH} \sigma$)	M_{BH}	4.86 ± 0.35	8.15 ± 0.05	0.45	0.53		
BCES(σM_{BH})	σ	6.94 ± 0.51	8.32 ± 0.07	0.54	0.64		
44 E-Type Galaxies							
BCES(<i>Bisector</i>)	<i>Symmetric</i>	6.69 ± 0.59	8.25 ± 0.10	0.30	0.43	} 0.82	0.80
BCES($M_{BH} \sigma$)	M_{BH}	6.05 ± 0.67	8.32 ± 0.10	0.29	0.41		
BCES(σM_{BH})	σ	7.47 ± 0.69	8.16 ± 0.12	0.32	0.47		
Galaxies with and without a bar							
50 Barred Galaxies							
BCES(<i>Bisector</i>)	<i>Symmetric</i>	5.30 ± 0.54	8.14 ± 0.10	0.45	0.53	} 0.65	0.61
BCES($M_{BH} \sigma$)	M_{BH}	3.97 ± 0.59	7.97 ± 0.10	0.43	0.49		
BCES(σM_{BH})	σ	7.86 ± 1.30	8.48 ± 0.19	0.61	0.71		
87 Non-Barred Galaxies							
BCES(<i>Bisector</i>)	<i>Symmetric</i>	6.16 ± 0.42	8.28 ± 0.06	0.40	0.51	} 0.86	0.86
BCES($M_{BH} \sigma$)	M_{BH}	5.57 ± 0.43	8.30 ± 0.06	0.40	0.49		
BCES(σM_{BH})	σ	6.88 ± 0.45	8.25 ± 0.07	0.44	0.55		

Table 3 continued

Table 3 (*continued*)

Regression	Minimization	α	β	ϵ	$\Delta_{rms BH}$	r	r_s
			(dex)	(dex)	(dex)		
(1)	(2)	(3)	(4)	(5)	(6)	(7)	(8)
Galaxies with and without an AGN							
41 AGN host Galaxies							
BCES(<i>Bisector</i>)	<i>Symmetric</i>	6.26 ± 0.49	8.21 ± 0.09	0.55	0.63	} 0.83	0.79
BCES($M_{BH} \sigma$)	M_{BH}	5.37 ± 0.51	8.16 ± 0.09	0.53	0.60		
BCES(σM_{BH})	σ	7.48 ± 0.66	8.28 ± 0.10	0.63	0.72		
96 Galaxies without AGN							
BCES(<i>Bisector</i>)	<i>Symmetric</i>	5.92 ± 0.31	8.30 ± 0.05	0.37	0.48	} 0.87	0.88
BCES($M_{BH} \sigma$)	M_{BH}	5.43 ± 0.33	8.29 ± 0.05	0.37	0.46		
BCES(σM_{BH})	σ	6.51 ± 0.33	8.30 ± 0.05	0.39	0.51		

NOTE— Columns: (1) Type of regression performed. (2) The coordinate direction in which the offsets from the regression line is minimized. (3) Slope of the regression line. (4) Intercept of the regression line. (5) Intrinsic scatter in the $\log(M_{BH})$ -direction (using Equation 1 from [Graham & Driver 2007](#)). (6) Total root mean square (rms) scatter in the $\log(M_{BH})$ -direction. (7) Pearson correlation coefficient. (8) Spearman rank-order correlation coefficient.

Table 4. Regression Lines Including All 143 Galaxies With Velocity Dispersions [$\log(M_{BH}/M_{\odot}) = \alpha \log(\sigma/200) + \beta$]

Category	Number	α	β	ϵ	$\Delta_{rms BH}$	r	r_s
			(dex)	(dex)	(dex)		
(1)	(2)	(3)	(4)	(5)	(6)	(7)	(8)
Early-Type Galaxies	95	5.05 ± 0.26	8.37 ± 0.04	0.33	0.44	0.90	0.87
Late-Type Galaxies	48	4.47 ± 0.80	8.04 ± 0.15	0.67	0.70	0.56	0.46
All Galaxies	143	5.29 ± 0.32	8.30 ± 0.04	0.50	0.58	0.86	0.86
Sérsic Galaxies	108	4.83 ± 0.35	8.22 ± 0.06	0.52	0.59	0.80	0.77
Core-Sérsic Galaxies	35	8.50 ± 1.10	7.91 ± 0.20	0.25	0.46	0.73	0.65
Galaxies with a disk (ES, S0, Sp-types)	98	4.90 ± 0.38	8.21 ± 0.06	0.54	0.60	0.79	0.76
Galaxies without a disk (E-type)	45	5.41 ± 0.66	8.40 ± 0.10	0.31	0.42	0.88	0.82
Barred Galaxies	52	4.05 ± 0.54	8.01 ± 0.10	0.45	0.51	0.74	0.66
Non-Barred Galaxies	91	5.46 ± 0.34	8.36 ± 0.06	0.48	0.55	0.86	0.86
AGN host Galaxies	42	5.23 ± 0.75	8.20 ± 0.08	0.62	0.67	0.82	0.81
Galaxies without AGN	101	5.26 ± 0.28	8.34 ± 0.05	0.44	0.52	0.87	0.87

NOTE— Columns: (1) Subclass of galaxies. (2) Number of galaxies in a subclass. (3) Slope of the line obtained from the BCES(BISECTOR) regression. (4) Intercept of the line obtained from the BCES(BISECTOR) regression. (5) Intrinsic scatter in the $\log(M_{BH})$ -direction (using Equation 1 from [Graham & Driver 2007](#)). (6) Total root mean square (rms) scatter in the $\log(M_{BH})$ direction. (7) Pearson correlation coefficient. (8) Spearman rank-order correlation coefficient.

Table 5. Luminosity versus Velocity Dispersion [$\log(L) = \alpha \log(\sigma/200) + \beta$]

Regression	Minimization	α	β	ϵ	$\Delta_{rms L}$	r	r_s
			(dex)	(dex)	(dex)		
(1)	(2)	(3)	(4)	(5)	(6)	(7)	(8)
V-band							
97 Core-Sérsic ETGs							
BCES(<i>Bisector</i>)	<i>Symmetric</i>	4.86 ± 0.54	8.52 ± 0.07	0.30	0.37	}	0.52 0.53
BCES($L \sigma$)	L	3.38 ± 0.48	8.70 ± 0.06	0.28	0.32		
BCES(σL)	σ	8.55 ± 1.53	8.08 ± 0.19	0.44	0.58		
80 Sérsic ETGs							
BCES(<i>Bisector</i>)	<i>Symmetric</i>	2.44 ± 0.18	8.41 ± 0.04	0.28	0.31	}	0.73 0.69
BCES($L \sigma$)	L	1.93 ± 0.18	8.35 ± 0.04	0.27	0.29		
BCES(σL)	σ	3.30 ± 0.36	8.51 ± 0.05	0.35	0.38		
3.6 μm							
24 Core-Sérsic ETGs							
BCES(<i>Bisector</i>)	<i>Symmetric</i>	5.16 ± 0.53	8.56 ± 0.08	0.00	0.19	}	0.86 0.76
BCES($L \sigma$)	L	5.48 ± 0.70	8.51 ± 0.11	0.00	0.20		
BCES(σL)	σ	4.86 ± 0.47	8.60 ± 0.07	0.00	0.18		
42 Sérsic ETGs							
BCES(<i>Bisector</i>)	<i>Symmetric</i>	2.97 ± 0.43	8.72 ± 0.07	0.33	0.36	}	0.61 0.61
BCES($L \sigma$)	L	2.10 ± 0.40	8.68 ± 0.06	0.32	0.33		
BCES(σL)	σ	5.04 ± 0.92	8.81 ± 0.09	0.49	0.53		
24 LTGs (All Sérsic)							
BCES(<i>Bisector</i>)	<i>Symmetric</i>	2.10 ± 0.41	8.90 ± 0.09	0.17	0.20	}	0.70 0.68
BCES($L \sigma$)	L	1.64 ± 0.44	8.83 ± 0.10	0.16	0.18		
BCES(σL)	σ	2.89 ± 0.42	9.03 ± 0.08	0.21	0.25		

NOTE— Columns: (1) Type of regression performed. (2) The coordinate direction in which the offsets from the regression line is minimized. (3) Slope of the regression line. (4) Intercept of the regression line. (5) Intrinsic scatter in the $\log(L)$ -direction (using Equation 1 from [Graham & Driver 2007](#)). (6) Total root mean square (rms) scatter in the $\log(L)$ -direction. (7) Pearson correlation coefficient. (8) Spearman rank-order correlation coefficient.

This figure "orcid-ID.png" is available in "png" format from:

<http://arxiv.org/ps/1908.06838v2>